DEPARTMENT OF PHYSICS
UNIVERSITY OF JYVÄSKYLÄ
RESEARCH REPORT No. 1/2011

DIFFUSION IN EVOLVING ENVIRONMENT: MONTE CARLO STUDIES OF DISCRETE MODELS

BY
JANNE JUNTUNEN

Academic Dissertation
for the Degree of
Doctor of Philosophy

To be presented, by permission of the
Faculty of Mathematics and Natural Sciences
of the University of Jyväskylä,
for public examination in Auditorium FYS-1 of the
University of Jyväskylä on February 5, 2011
at 12 o'clock noon

Jyväskylä, Finland
January 2011

Preface

Finally this academic jorney that have sometimes felt like a walk in a wet swamp is, at least temporarily over. The feet have met a solid ground.

The work reviewed in this Thesis has been carried out at the Department of Physics in the University of Jyväskylä during the years 2005-2010. The journey has take more time than anticipated but in the end the time has been spent learning the magic of doing and understanding physics. I am greatly in dept to Docent Juha Merikoski who introduced the world of computational physics and stochastic modelling to me. The collaboration with Dr. Otto Pulkkinen has revealed the usefulness of the concept of random walks as one of the main tools in stochastic modelling.

During these years I have had the pleasure to spent my time in and out of department with phycisists in many fields of physics. Especially discussions with docent Jari Hyväluoma and Dr. Keijo Mattila have revealed many aspects of natural sciences and physics, which has kept my eyes open and guaranteed a very comprehensive picture of physics and how it has been done and is done nowadays. The athmosphere of my "'coffee lounge"', the Hard Humppa Cafe, greated by Dr. Viivi Koivu, Mr. Tuomas Turpeinen, Mr. Mikko Voutilainen and Mr. Lasse Miettinen has provided a place to relax and forget physics. I am greatly in dept also to Mr. Juha Sorri and Mr. Topi Kähärä and those nonmentioned persons that have sometimes participated some tournament of Atomi Fragor (Atomin Pamaus), "Fulgur cum vides, zero est". For creating an open and truly inspirated environment I must thank the Deparment of Physics entirely.

Finally, I wish to thank my family that couraged me to study as far as I can and most of all my wife Terhi for always motivating me to finish my thesis as fast I can.

Jyväskylä, January 2011

Janne Juntunen

Abstract

Diffusion in a dynamic environment is studied by Monte Carlo simulations. The Thesis consists of an introductory part and four publications, in which diffusion in evolving environments is studied. A general theoretical framework is presented in a separate chapter of the introductory part.

The spatiotemporal behavior and stationary properties of environments, the area between two interfaces driven towards each other and zero-range processes, is studied in detail in order to understand the time and length scales relevant to the dynamics of such environments. Special emphasis is in the finite size and crossover effects. The main observation concerning the two interface scenario is the non-monotonic behavior of the roughness of the interfaces, which is a genuine finite size effect. By analyzing the behavior of the largest cluster in the zero-range process we find that we can determine the effective critical density $\rho_c(L)$ that is a prominent factor in stationary and dynamical quantities. Below the density $\rho_c(L)$ the collective diffusion coefficient is found to be larger than the diffusion coefficient for the center of mass movement and above it smaller, reflecting the crossover at $\rho_c(L)$.

Tracer diffusion between two interfaces driven towards each other is found to depend strongly on the bubble dynamics. In the weak drive limit the probability of the particle inside the bubble is found to control diffusion, while in the strong drive limit the probability that a particle makes a jump during the bubble life time explains the behavior of the diffusion coefficient. These two scaling limits are not compatible. One of the key findings is the effect on the diffusion coefficient due to the microscopic coupling of the particle and interfaces. In the case of a driven exclusion process between two interfaces the particle current depends on several properties of the interfaces. As for the zero-range process and for single-particle diffusion between the interfaces, the dynamics of the environment strongly controls the transport.

Author's address Janne Juntunen
Department of Physics
University of Jyväskylä
Finland

Supervisor Docent Juha Merikoski
Department of Physics
University of Jyväskylä
Finland

Reviewers Professor Erik Aurell
Department of Computational Biology
Royal Institute of Technology
Stocholm
Sweden

Docent Ismo Koponen
Department of Physics
University of Helsinki
Finland

Opponent Professor Mikko Alava
Department of Applied Physics
Aalto University School of Science and Technology
Finland

List of Publications

I Janne Juntunen, Otto Pulkkinen and Juha Merikoski, *Roughness of two nonintersecting one-dimensional interfaces* Phys. Rev. E **76**, 041607 (2007)

II Janne Juntunen, Otto Pulkkinen and Juha Merikoski, *Finite-size effects in dynamics of zero-range processes* Phys. Rev. E **82**, 031119 (2010)

III Janne Juntunen and Juha Merikoski, *Diffusion between evolving interfaces* J. Phys: Cond. Matt. **22**, 465402 (2010)

IV Janne Juntunen and Juha Merikoski, *Two dimensional exclusion process between rough interfaces*, To appear in J. Phys: Conf. Ser. (2010)

The author of this Thesis has done all simulations and all data analysis of articles I-IV except the finite-size analysis in article I. The author has contributed to defining and testing the concepts and quantities used to characterize the dynamics of the studied systems. The author has written the first drafts of articles II and III, written article IV and participated in writing article I.

Contents

1 Introduction

Diffusion is an ubiquitous phenomenon in nature. This in part explains why diffusion is one of the most frequently studied phenomena in physics. Everyday examples of diffusion are numerous and one of the best known examples is heat transfer by conduction in metals. Informally, diffusion is a process smoothing out concentration differences in a system. More fundamentally, diffusion is a consequence of the basic laws of the thermodynamics, in particular it arises as a consequence of the second law of thermodynamics: The entropy of a closed system will increase with time.[1]

Understanding diffusion in various situations has been and will probably be in a significant role in the development of many technological innovations. One example of the advances of understanding diffusion is the progress done in manufacturing transistors. Understanding of the point-defect mediated diffusion in a material has enabled transistors so small that they can be considered to be in many applications essentially two or even one dimensional without any critical deficiencies. In addition, the fact that transistors are manufactured of materials which have some kind of a structure gives a possibility to consider the system as a discrete finite size lattice on which the diffusing particles moves.

Historically, in condensed-matter physics the fact that some thermal properties must be calculated for model systems of finite size, has often been considered to be a problem. It is true that a model system of finite size can behave differently from a similar system of a macroscopic or hydrodynamical size. But the Nature strikes back. It is well documented that, for example, gold behaves differently in different scales. It is common knowledge that gold is a chemically stable element. However, when considering clusters of only a few dozen gold atoms it suddenly is not stable, in fact it is catalytic. Finite-size effects can be divided in two distinct categories, namely physical and non-physical ones. The first category involves phenomena due to a small or even nanoscale size and the second one includes other reasons such as artifacts of the models or methods. By Monte Carlo (MC) simulations only systems of finite size are attainable because of the very nature of the method. Theoretical analysis methods have been developed to overcome this difficulty, in particular finite-size scaling [1] being the tool to transfer MC results obtained for small sizes into results valid in the hydrodynamical limit. Often the change of a system which displays a finite size effect into a system large enough so that it appears to be hydrodynamical is not a rapid

[1] Entropy is a measure of disorder. It describes how much energy that was originally stored in the system can be extracted from it to perform useful work at later instant of time.

one. Indeed one can argue that the system is in the so called crossover region in which it displays behavior characteristic of both phases.

An often used and a powerful frame for studying diffusion is provided by the theory of random walks. The variations of the random walk model are numerous. One common feature of those models is that they satisfy the Markov property *i.e.* the behavior in the past does not affect the behavior in the future. Only few attempts of understanding random walks out of the Markovian framework have been considered. This of course is forgivable since there is no general theoretical framework beyond the Markovian one [2]. One of the most relevant and useful random walk models for the purposes of this Thesis is the continuous time random walker (CTRW) first considered in detail by Montroll in the 70's [3]. One of the advantages of CTRW is that the randomness of the environment is easily taken into account.

Even though the problem of random walks in a random environment (RWRE) has a long history, and after the early results in the 1970s [4, 5, 6], a vast amount of information have accumulated, they are usually studies were randomness has been considered to manifest itself as non-homogeneous transition rates [7, 8]. In cases were the transition rates are themselves a result of a random walks are described by the Sinai model [9]. However, these studies have quite often been limited to systems, where the close environment of the diffusive particle is stationary and the geometry is not restricted. Recently there has been interest towards models of diffusion where the geometry is restricted [10] and the force that causes the motion of the particle depends on time and place [11]. This can be interpreted as particle diffusion in a random dynamic environment. It has been noticed that fluctuations of the environment can cause an otherwise nondiffusive motion to change into diffusive [12].

The outline of this Thesis is as follows. In Chapter 2 we characterize diffusion and how it can be modeled. In Chapter 3 we introduce the models studied and discuss the Monte Carlo methods used. In Chapter 4 we review our main results for diffusion in evolving and restricted environments. The final chapter comprises a brief summary.

2 Diffusion and random walks

2.1 Diffusion

Diffusion as a concept is ambiguous. This question is actually one focus of our interest. If we consider a physical system at a microscopic level we can either consider an individual particle or a collection of them. Naturally the behavior of a single particle is not necessarily similar to the behavior of a collection of them. Therefore we must consider these scenarios separately. If we consider a single particle moving among others we are studying tracer diffusion. When our focus is on how the system behaves as a group of particles, collective diffusion is under consideration.

2.1.1 Tracer diffusion

A classical example of diffusion is the motion of a particle suspended in a liquid. The very first time this kind of motion was observed in 1828 by botanist Robert Brown when he studied pollen of different plants and observed that when placed in water the pollen particles were in constant irregular motion. Nowadays this Brownian motion is understood to be motion of colloidal particles in a liquid and to result from random molecular collisions with liquid molecules.

The first explanation for such motion was given by Einstein in 1905 [13, 14]. The idea of using a random walk picture as a tool for analyzing Brownian motion is quite remarkable when considering the fact that the concept of random walk explicitly had appeared in the literature in the same year [15].

In a situation where there are no mutual interactions between Brownian particles a simple theory for Brownian motion is the Langevin equation:

$$m\frac{d}{dt}\vec{v}(t) = -\nu m\vec{v}(t) + \vec{F}(t), \tag{2.1}$$

where m and $\vec{v}(t)$ are mass and the velocity of the particles at time t, respectively, $\vec{F}(t)$ is the driving random force for the Brownian particle that arises from the thermal motion of fluid molecules and ν is the friction coefficient. This approach is on a solid ground as long as the Markovian limit has been reached. Basically this requires that

the time scales of the particle and fluid molecules are decoupled, otherwise friction is a function of time and results in memory effects of the diffusing particle.

The description of Brownian motion is a good example of tracer diffusion, *i.e.* diffusion of individual particles among others. One of the most important results of Einstein's paper [13] and one of the most straightforward way to determine the tracer diffusion coefficient D_T is the mean square displacement

$$\langle \Delta X^2(t) \rangle = 2dD_T t^\alpha, \qquad \alpha = 1 \tag{2.2}$$

where d is the dimension in which the diffusion process occurs and t is the length of the time interval. For $\alpha < 1$ system is said to be subdiffusive and for $\alpha > 1$ superdiffusive [16].

2.1.2 Collective diffusion

As discussed already in Chapter 1, diffusion is a process which tends to equalize the concentration within the system. However, from the concept of Brownian motion or tracer diffusion it may be difficult to see the connection with this. The equilibration of matter density is best understood if one considers the motion of a larger collection of particles. For this kind of evolution the commonly used term is collective diffusion the corresponding coefficient being D_C.

A natural description of transport coefficients is the Green-Kubo (linear) response function formalism [17, 18]. In the Green-Kubo formalism every transport coefficient is expressed via time correlations of some current. For collective diffusion

$$D_C = K \int_0^\infty dt \langle \vec{j}(t) \cdot \vec{j}(0) \rangle, \tag{2.3}$$

where $\vec{j}(t)$ is the particle current. In general, the explicit forms of the flux and the so-called thermodynamic factor in front of the correlator depend on the transport coefficient under consideration [17]. The collective diffusion coefficient (a tensor in the anisotropic case) can then be written as a product of two factors, namely K and the center of mass diffusion coefficient D_{CM}, as

$$D_C = K D_{CM}, \tag{2.4}$$

where D_{CM} is obtained from equations analogous to (2.2-3). The factor K arises from the particle number fluctuations in equilibrium described by the grand-canonical ensemble, $K = \langle (N - \langle N \rangle)^2 \rangle / \langle N \rangle$, assuming Gaussian fluctuations around the most probable particle density. The factor K is inversely proportional to the compressibility. Equation (2.4) thus reveals one major difference between tracer diffusion (of single

particle or the center of mass) and collective diffusion. The second important difference results from cross correlations:

$$\frac{D_C}{D_{CM}} = \frac{N}{\langle(\Delta N)^2\rangle}\Big(1 + \frac{\int_0^\infty dt \sum_{i\neq j}\langle\vec{v}_i(0)\cdot\vec{v}_j(t)\rangle}{\int_0^\infty dt \sum_i\langle\vec{v}_i(0)\cdot\vec{v}_i(t)\rangle}\Big),$$

where v_i are the velocities of individual particles.

2.1.3 Hydrodynamic equations

Above diffusion processes were considered in a microscopic scale, arising from particle motion. However in a hydrodynamical scale a description based on differential equations is a more proper approach.

In the hydrodynamical treatment of diffusion the starting point is the postulate that the particle density $\rho(\vec{r},t)$ is a conserved variable. The second necessary requirement is an explicit form for the driving force [17]. Usually this is fulfilled by assuming that the mass transport across a certain unit area is proportional to the gradient of the particle density normal to unit area. These two postulates are described by the continuity equation,

$$\frac{\partial\rho}{\partial t} + \nabla\cdot\vec{j} = 0, \tag{2.5}$$

and the phenomenological Fick's first law for the particle current density $\vec{j}(\vec{r},t)$,

$$\vec{j}(r,t) = -D_C(\rho)\nabla\rho(\vec{r},t). \tag{2.6}$$

By combining these two equations, one obtains

$$\frac{\partial\rho}{\partial t} = \nabla\cdot D_C(\rho)\nabla\rho(\vec{r},t), \tag{2.7}$$

which is a non-linear partial differential equation, which often is not analytically solvable. Usually however additional approximation can be done and by assuming independence of the diffusion coefficient on density resulting in

$$\frac{\partial\rho}{\partial t} = -D_C\nabla^2\rho(\vec{r},t), \tag{2.8}$$

which is the diffusion equation that can be often solved exactly. Similar hydrodynamic equations describe also tracer diffusion, with ρ then interpreted as a probability density [19].

In Eq. (2.3) we expressed a way to calculate the collective diffusion coefficient D_C. However the computational determination of D_C from Eq. (2.3) is difficult. Since the thermodynamical factor in Eq. (2.4) is proportional to density fluctuations, a natural starting point for a more practical approach is provided by the density autocorrelation function [17, 18]

$$S(\vec{r}, \vec{r}', t) = \langle \delta\rho(\vec{r}, t)\delta\rho(\vec{r}', 0)\rangle, \tag{2.9}$$

where $\delta\rho(\vec{r}, t) = \rho(\vec{r}, t) - \langle\rho\rangle$. Inserting this autocorrelation function in the diffusion equation (2.8) we obtain a diffusion equation for the autocorrelation function, *i.e.* $\partial_t S(\vec{r}, t) = -D_C\nabla^2 S(\vec{r}, t)$. From the solution of the diffusion equation the density fluctuations are found to decay as

$$S(\vec{k}, t) = S(\vec{k}, 0)\exp(-\vec{k}\cdot D_C\cdot\vec{k}t). \tag{2.10}$$

2.2 Random walk models of diffusion

A natural framework for modeling diffusion is provided by the theory of random walks [15]. Especially Brownian motion can be described with it. From the perspective of this Thesis the most relevant model of random walks is the continuous time random walk (CTRW) on a lattice introduced by Montroll in the 70's [3]. The general CTRW model is based on a the idea that the jump length distribution and the waiting time distribution are drawn from a common distribution $\psi(t, \Delta x)$ from which the jump length and waiting distribution are

$$\lambda(\Delta x) = \int_0^\infty dt\,\psi(t, \Delta x) \qquad \phi(t) = \int_0^\infty dx\,\psi(t, \Delta x).$$

If the waiting time and the jump length are independent random variables, the common distribution can be written in the decoupled form $\psi(t, \Delta x) = \lambda(\Delta x)\phi(t)$. If both are coupled $\psi(t, \Delta x) = \lambda(\Delta x|t)\phi(t)$ or $\psi(t, \Delta x) = \phi(t|\Delta x)\lambda(\Delta x)$, a jump of certain length will cost a certain time and vice a versa. In what follows we consider the origin of correlations in the diffusive motion.

2.2.1 General solution for CTRW on a lattice

We use the recursion relation approach to solve the general CTRW on a lattice. The notations obey those of Ref. [20]. For simplicity let us assume that the particle has performed its latest transition at time $t = 0$. Then $\psi_{n,m}(t)$ is the probability density that the particle jumps at time t from site m to site n after waiting time t on m. It must be positive semidefinite and it must be normalized, $\sum_n \int_0^\infty dt'\psi_{n,m}(t') = 1$.

Since the tracer diffusion coefficient is usually obtained from the mean-square displacement via Eq. (2.2) the understanding of tracer diffusion is reduced to the understanding of the probability distribution function of the location of the particle at time $t > 0$ with the condition that at time $t = 0$ it was in a given lattice site l *i.e* the conditional probability $P(n, t|l, 0)$.

Let $Q_\nu(n, t')$ be the probability density that the particle has performed its νth transition at time t and reached site n. Recursively this can be written as

$$Q_\nu(n, t') = \sum_m \int_0^{t'} dt^* \psi_{n,m}(t' - t^*) Q_{\nu-1}(m, t^*). \tag{2.11}$$

This relation however is valid only for $\nu \geq 2$ since the first transition has to be treated differently. By summing over ν *i.e*, the numbers of transitions in which the particle has moved to n we obtain the probability density that site n is occupied by a transition at time t'

$$Q(n, t') = \sum_\nu Q_\nu(n, t'). \tag{2.12}$$

This equation can obviously be written for all lattice sites, not only for n. The recursion for $Q(n, t')$ is similar to Eq. (2.11) for $Q_\nu(n, t')$, see the Appendix for details. The probability $P(n, t|l, 0)$ is thus related to $P(n, t')$. If the particle arrived in site n at t', then the probability that it still is at the same site depends of the probability that no further jumps occurs between t' and t. In case where no transitions occurred at all, the particle was already at site n at time $t = 0$. Finally, the required probability in Fourier-Laplace space is

$$\tilde{P}(k, s) = \frac{1 - \tilde{h}(0, s) + \tilde{h}(k, s) - \tilde{\psi}(k, s) + \tilde{h}(0, s)\tilde{\psi}(k, s) - \tilde{h}(k, s)\tilde{\psi}(0, s)}{s(1 - \tilde{\psi}(k, s))}, \tag{2.13}$$

which get simplified for a separable CTRW to

$$\tilde{P}(k, s) = \frac{1 - \tilde{h}(0, s) + \tilde{\lambda}(k)[\tilde{h}(s) - \tilde{\phi}(s)]}{s(1 - \tilde{\lambda}(k)\tilde{\phi}(s))}, \tag{2.14}$$

comprised of products of spatial and temporal factors and $\tilde{\psi}(0, s) = \tilde{\psi}(s) = \tilde{\phi}(s)$. If we consider a stationary ensemble, the waiting time distribution for the first jump is the conditional probability to wait time t even though it has already waited time τ. The Fourier-Laplace transform of this probability is

$$\tilde{h}(k, s) = \frac{\tilde{\psi}(k, 0) - \tilde{\psi}(k, s)}{\bar{t}s}, \tag{2.15}$$

where $\bar{t}$ is the expected waiting time of the particle.

Finally we obtain the conditional probability in a stationary ensemble

$$\tilde{P}(k,s) = \frac{1}{s} + \frac{1}{\bar{t}s^2}\frac{[1-\tilde{\psi}(0,s)][\tilde{\psi}(k,0)-1]}{1-\tilde{\psi}(k,s)}. \tag{2.16}$$

This illuminating result is for the coupled case. For the decoupled case in the denominator $\tilde{\psi}(k,s) = \tilde{\lambda}(k)\tilde{\phi}(s)$. If the system is prepared on $t = 0$ so that it evolves according to $\psi_{n,m}(t)$ it follows that $h_{n,m}(t) = \psi_{n,m}(t)$. In fact if the waiting-time distribution (WTD) has no memory, then $h_{n,m}(t) = \psi_{n,m}(t)$ is always true without the assumption of preparation of the system on $t = 0$.

Replacing $\tilde{h}(k,s)$ by $\tilde{\psi}(k,s)$ in Eq. (2.13) one obtains

$$\tilde{P}(k,s) = \frac{1-\tilde{\psi}(0,s)}{s}\frac{1}{1-\tilde{\psi}(k,s)} \tag{2.17}$$

for a coupled distribution. For the decoupled case we have in the denominator $\tilde{\psi}(k,s) = \tilde{\lambda}(k)\tilde{\phi}(s)$. The decoupled result is called the Montroll-Weiss equation and it is an exact solution of the problem in the Fourier-Laplace space.

2.2.2 Properties of RW diffusion

In a case where the characteristic function of the associated density function is known, the moments can be obtained from $\langle x^n\rangle = \lim_{k\to 0}(-i)^n d^n f_X(x)/dk^n$ and the mean-square displacement of the particle is thus

$$\langle x^2\rangle(s) = -\nabla_k^2 \tilde{P}(k,s)|_{k=0}, \tag{2.18}$$

where for simplicity and for the purposes of this work we consider one-dimensional motion. Now using Eq. (2.18) with Eq. (2.16) we obtain the tracer diffusion coefficient in the general case through

$$\langle x^2\rangle(s) = -\frac{1}{\bar{t}s^2}(1-\tilde{\phi}(s))\Big(\frac{\tilde{\lambda}''(0)}{1-\tilde{\phi}(s)} + 2\frac{\tilde{\lambda}'(0)\tilde{\psi}'(0,s)}{(1-\tilde{\phi}(s))^2}\Big). \tag{2.19}$$

Since $\tilde{\lambda}'(0) = -i\langle\Delta x\rangle$ and $\tilde{\lambda}''(0) = -\langle(\Delta x)^2\rangle$ and the terms $\tilde{\psi}^n(0,s)$ are of the form

$$\langle(\Delta x)^n(s)\rangle = \tilde{\psi}^n(0,s) = (-i)^n \int \phi(t)\langle(\Delta x)^n(t)\rangle e^{-st}dt, \tag{2.20}$$

for $\langle x^2\rangle(s)$ we obtain its final form in the Fourier-Laplace domain,

$$\langle x^2\rangle(s) = \frac{1}{\bar{t}s^2}\Big(\langle(\Delta x)^2\rangle + 2i\frac{\langle(\Delta x)\rangle\langle(\Delta x(s))\rangle}{(1-\tilde{\phi}(s))}\Big). \tag{2.21}$$

For the decoupled case in the numerator $\langle x\rangle\langle x(s)\rangle = \langle x\rangle^2\phi(s)$ and hence the result can be presented as

$$\langle x^2\rangle(s) = \langle n(s)\rangle\langle(\Delta x)^2\rangle + \langle n(s)(n(s)-1)\rangle\langle(\Delta x)\rangle^2, \tag{2.22}$$

where $\langle n(s)\rangle$ is the Laplace transform of the expected number of steps taken during the time t (see Appendix).

If $\tilde{h}(k,s) = \tilde{\psi}(k,s)$ as it is for example in cases with exponential waiting times, we obtain for the decoupled case the same result as in Eq. (2.22) and for the coupled case

$$\langle x^2(s)\rangle = -\frac{\langle(\Delta x)^2(s)\rangle}{s(1-\tilde{\phi}(s))} - 2\frac{(\Delta x(s))^2}{s(1-\tilde{\phi}(s))^2}. \tag{2.23}$$

As we can see from Eqs. (2.21) and (2.23) the coupled versions of CTRW can not be developed further without an assumption of the forms of the waiting time distribution. However in the long time limit (small s) we can approximate Eq. (2.20) by

$$\langle(\Delta x)^n(s)\rangle = (-i)^n(\langle(\Delta x)^n\rangle - s\langle(\Delta x)^n t\rangle + \frac{s^2}{2}\langle(\Delta x)^n t^2\rangle + ...).$$

By substituting the approximation above to Eq. (2.21) we obtain

$$\langle x^2\rangle(s) = \frac{\langle(\Delta x)^2\rangle}{\bar{t}s^2} + 2\frac{\langle\Delta x\rangle^2}{s^3\langle t\rangle^2} - 2\frac{\langle\Delta x\rangle\langle\Delta xt\rangle}{s^2\langle t\rangle^2}$$

and for $h(t) = \psi(t)$ in the small s limit

$$\langle x^2\rangle(s) = \frac{\langle(\Delta x)^2\rangle}{\bar{t}s^2} - \frac{\langle(\Delta x)^2 t\rangle}{s\langle t\rangle} + 2\frac{\langle\Delta x\rangle^2}{s^3\langle t\rangle^2} - 4\frac{\langle\Delta x\rangle\langle\Delta xt\rangle}{s^2\langle t\rangle^2} + \frac{\langle\Delta xt\rangle^2}{s\langle t\rangle^2}.$$

In the non-driven situation, $\langle\Delta x\rangle = 0$, the motion of the particle is then purely diffusive $\langle x^2(t)\rangle = \langle(\Delta x)^2\rangle t/\bar{t}$, if the averages $\bar{t}$ and $\langle(\Delta x)^2\rangle$ exist. Here we assume their existence.

In Ref. [21] Klafter et al. considered the coupled version of the case $h(x,t) = \psi(x,t)$. By using the specific form

$$\psi(k,s) \sim 1 - C_1 s^\gamma - C_2 k^\beta$$

of the Fourier-Laplace transformed transition rate function $\psi(x,t)$. They found that $\langle x^2\rangle(t)$ diverges, if $0 < \beta < 2$ despite of the γ and if $0 < \gamma < 1$, $C_2 = \langle x^2\rangle/2$ and $\beta = 2$ $\langle x^2\rangle(t) \sim t^\gamma$. In the literature the cases where $\langle x^2\rangle$ is infinite are better known as Levy flights [21] and the case of spatiotemporal coupling of waiting times and jump length is known as Levy walks.

If the average waiting times $\bar{t}$ are finite or diverge mildly the models are ergodic. The importance of the ergodicity is that the ergodic hypothesis states that ensemble averages and time averages are equal in the limit of infinite measurement time. There are two requirements for the system to be ergodic. First, the phase space must be connected and the the occupation time must be equal to the fraction of the phase space volume occupied. Naturally CTRWs satisfy the first requirement. Problem arise when considering the second requirement. This requirement is typically broken in cases where each lattice site has a different WTD [22]. This weak ergodicity breaking was studied recently quite comprehensively for CTRW. Usually ergodic systems obey the Boltzmann distribution. In Ref. [23] a nonergodic statistical law for the nonergodic phase was found.

Above we have assumed that the waiting times and jump lengths are independent and identically distributed random variables. In Ref. [24] a general mathematical framework for nonindependent CTRWs was developed. However only certain type of nonindependency can be dealt with accurately and the results obtained lead to a diffusive behavior. In Ref. [25], however, it was found that if we allow correlations for λ or ϕ, *i.e.* memory, these correlations lead necessarily to anomalous diffusion. Spesifically, if waiting times are correlated by Gaussian statistics $\langle x^2 \rangle(t) \sim t^{2/3}$ while long-ranged correlations of waiting times by power law with $0 < \alpha \leq 2$ such that $\langle x^2 \rangle(t) \sim t^{\alpha/(\alpha+1)}$, correlations in jumps length produce superdiffusion. In both cases correlations cause a weak ergodicity breaking. We get back to ergodicity breaking in Section 3.5.4 where we consider sampling of quantities in numerical simulations.

3 Models

3.1 Zero-Range Process

The zero range process (ZRP) was first mentioned in the literature in the 70's as an example of an interacting Markov process [26]. Nowadays it is a central reference model when considering nonequilibrium systems in condensed-matter physics. Here a rather informal definition of it for the purposes of this work is given.

Even though majority of the analytical results concerning ZRP are obtained via grand-canonical analysis, in this Thesis we only consider canonical case. Informally, the canonical ZRP is a stochastic process on a lattice or graph containing L sites $i = 1, 2, \ldots, L$, with N identical particles. The dynamics of the ZRP is defined by a transition rate function $u_i(k_i)$. The dynamics occurs so that at each time step from a randomly chosen site i a particle jumps to site j with probability $u_i(k_i)$, where due to the zero-range property there is no dependence on j. The symbol k_i identifies the number of particles in lattice point i.

The vector formed by the set $\{k_i\}$ defines unambiguously a configuration m. The probability that the system is in configuration m in the stationary state is

$$P(m) = \frac{1}{Z(L,N)} \prod_{i=1}^{L} f_i(k_i), \tag{3.1}$$

where the function f_i is

$$f_i(k) = \begin{cases} \prod_{h=1}^{k} \frac{1}{u_i(h)} & , \text{if } k \geq 1 \\ 1 & , \text{if } k = 0. \end{cases} \tag{3.2}$$

The previous statement can be easily verified by showing that the probability distribution satisfies the detailed balance condition. The factor $Z(L,N)$ in Eq. (3.1) assures that the probability $P(\{m\}) = 1$ and it is therefore analogical with the partition function which appears in statistical mechanics. Here the partition function is

$$Z(L,N) = \sum_{k_i} \delta(\sum_{i=1}^{L} k_i - N) \prod_{i=1}^{L} f_i(k_i). \tag{3.3}$$

In this Thesis we study only one kind of transition rate functions. We focus on functions of the form

$$u(k) = u_0(1 + b/k) \tag{3.4}$$

which are sometimes called as Evans-type transition rates. With these transition rates, there is a continuous phase transition at the critical density

$$\rho_c = \frac{1}{b-2} \tag{3.5}$$

whenever $b > 2$. Even though the system is expected to be in a condensed phase whenever $b > 2$ and $\rho > \rho_c$, the behavior of the system in cases $2 < b < 3$ is expected to be different from cases $b > 3$.

In the condensed phase the particles form a homogeneous critical background and a macroscopic condensate, consisting of Z_1 particles with

$$Z_1 = L(\rho - \rho_c) \qquad \Rightarrow \qquad \tilde{Z}_1 = \frac{Z_1}{N} = 1 - \frac{\rho}{\rho_c}. \tag{3.6}$$

The results above are obtained via grand-canonical analysis and are not valid for small system sizes. Quite recently Evans et al. [27, 28] studied the condensation phenomena canonically. The main results of those papers are the finite-size scaling of the size distribution of the largest cluster $P(Z_1, N, L)$ and the probability $p(k_i)$ i.e. the probability that a randomly chosen site i has occupation k_i. Especially the analysis concerning $f(k) = Ak^{-\gamma} (\gamma > 2)$ is of interest to us since the Evans-type rates $u(k)$ lead to this form.

For $2 < \gamma < 3$ the occupation probability of a single site is

$$p(k) \approx f(k) \frac{V_\gamma(k/L^{1/(\gamma-1)})}{V_\gamma(0)} \tag{3.7}$$

and the size distribution of the largest cluster is

$$P(x, N, L) = \frac{1}{L^{1/(\gamma-1)}} V_\gamma\Big(\frac{x - L(\rho - \rho_C)}{L^{1/(\gamma-1)}}\Big). \tag{3.8}$$

The scaling function V_γ is highly symmetric around $z = 0$. For $\gamma > 3$

$$p(k) \approx f(k) \exp(-k^2/2 \cdot Z_1^2 L) \tag{3.9}$$

and

$$P(x, N, L) = \frac{1}{\sqrt{2\pi\Delta^2 L}} \exp\Big(-\frac{(x - (\rho - \rho_c)L)^2}{2\Delta^2 L}\Big). \tag{3.10}$$

This Gaussian form is valid over a scale $o(L^{2/3})$.

Even though the distributions for the size of the largest cluster (see Eqs.(3.8) and (3.10)) are for the generalized mass transport model (GMT) [29], the results apply to ZRP since it belongs to the universality class of GMT. One species ZRP can be generalized to the many species case [30]. Here we consider briefly two species ZRP.

In a two species ZRP there are N particles of species A and M particles of species B. The particles of species A make nearest-neighbor hops with a rate $u(n,m)$ and particles of species B with a rate $v(n,m)$. In Ref. [30] it has been shown that if the hopping rates satisfy the condition

$$\frac{u(n_l,m_l)}{u(n_l,m_l-1)} = \frac{v(n_l,m_l)}{v(n_l-1.m_l)},$$

the system has a factorized steady state. Basically, this restriction says that both species are independent or their dynamics depend on each other in the given way. For our purposes, however, the factorization condition is not important.

3.2 Exclusion process

The asymmetric exclusion process (ASEP) is a continuous time Markov process of interacting particles on a lattice. Its dynamics is described by two simple rules: A particle at lattice point i waits an exponential time with parameter α (independently of all other particles) and then it chooses its movement with probability $p(i,j)$. If the lattice site j is empty at that time the particle moves to it, while if it is occupied the particle remains at i and restarts its clock.

In the one dimensional case the allowed jumps are one step to the right, $p(i,i+1)=p$, or one step to the left $p(i,i-1)=1-p=q$. The symmetric condition is $p=q$ so there is no net drift of particles. The special cases $p=1$ (particles hop only to the right) or $q=1$ (particles hop only to the left) are called the T(totally)ASEP. Generalization of 1D ASEP to higher dimensions is trivial. One dimensional exclusion process can be mapped onto the ZRP, however this mapping is not one-to-one [31].

In the continuum limit the asymmetric exclusion process (ASEP) is known to obey the Burgers equation [32]

$$\frac{\partial u}{\partial t} + u\frac{\partial u}{\partial x} = \nu\frac{\partial^2 u}{\partial x^2}, \tag{3.11}$$

where u is velocity and ν is the viscosity. The general case can be linearized by the Cole-Hopf substitution $u = -2\nu\frac{1}{\phi}(\frac{\partial\phi}{\partial x})$ and one the obtains the diffusion equation $\partial_t u = \nu\partial_x^2 u$.

3.3 Solid-On-Solid models

First of all solid-on-solid (SOS) models describe the growth or evolution of an interface defined on a lattice. Another common feature of all SOS models is that they describe only single valued interfaces and they usually restrict the difference between the neighboring sites. Here we consider only one particular SOS model namely the Body-Centered Solid-On-Solid model (BCSOS). It can be mapped onto ASEP [33] and via ASEP further onto ZRP [31].

In the BCSOS model of a single one-dimensional interface [34], the location or the height of the interface is described by a function $h(x,t)$ such that, for every lattice site $x = 1, .., L$ and $t \geq 0$,

$$h(x+1,t) - h(x,t) = \pm 1. \tag{3.12}$$

Due to these restrictions on local configurations, only two kinds of processes, adsorption and desorption, are available and the growth of the interface follows simple rules. In discrete time, if at some time step a randomly chosen lattice point x is a local minimum, then $h(x,t)$ increases (adsorption) by two with probability p, and if the chosen point is a local maximum, then it decreases (desorption) by two with probability q. In our continuous-time simulations (see Section 3.5.3), the parameters p and q correspond to respective transition rates per unit time.

The BCSOS2 model consists of two one dimensional BCSOS interfaces h_1 and h_2 interacting with each other, see figure 1 of Article I. The coupling between them is produced by demanding that the interfaces can not intersect:

$$h_1(x,t) \geq h_2(x,t) \quad \text{for all} \quad x,t. \tag{3.13}$$

In all cases considered here, we impose periodic boundary conditions $h_k(x,t) \equiv h_k(x+L,t)$ for $k = 1, 2$.

In this model, there are four parameters, which describe the dynamics of the interfaces in all possible situations, (p_1, q_1, p_2, q_2), defining the transition rates for the interfaces h_1 and h_2, respectively. In a symmetric case the behavior of the BCSOS2 is controlled by the driving parameter f

$$f = p_2/q_2. \tag{3.14}$$

We consider also the difference and sum processes defined via

$$h_\pm(x,t) = h_1(x,t) \pm h_2(x,t) \tag{3.15}$$

The interfaces $h_\pm$ are of the restricted solid-on-solid (RSOS) type [34], obeying

$$h_\pm(x+1,t) - h_\pm(x,t) = -2, 0, +2. \tag{3.16}$$

The non-crossing condition of Eq. (3.13) is equivalent to

$$h_-(x,t) \geq 0. \tag{3.17}$$

To characterize the statistical properties of interfaces h_1 and h_2, and the sum and difference processes h_+ and h_-, we use their roughness or width [34] defined as

$$W_k(t) = \sqrt{\langle |h_k(x,t) - \bar{h}_k(t)\rangle|^2\rangle} \tag{3.18}$$

Here $k = 1, 2, +, -$ and $\bar{h}_k(t)$ is the spatially averaged height of the interface configuration at time t, and the angle brackets denote ensemble average, *i.e.* average over independent simulations.

Since the BCSOS model is defined in a discrete finite size lattice of length L, a natural question is what happens to roughness W if one changes the system size. Let assume that the interfaces is as smooth as it can be *i.e* $h(x, t = 0) = 1$ if $x = 2n$ where $n \in N$ and otherwise zero. For all system sizes the width $W(t) \sim t^\beta$ until some characteristic time $t_{sat} \sim L^z$ and it saturates to the value $W^s \sim L^\alpha$. With the help of these two notions we can guess the form of the scaling function for the roughness, $W(L,t)/W_{stat} \sim f(\frac{t}{t_x})$, and thus obtain the well known Family-Vicsek scaling relation $W(L,t) \sim L^\alpha f(\frac{t}{t_x})$, where t_x is the time where $W(t > t_x)$ becomes constant [35] .

The BCSOS2 model could have also been described by the language of the ASEP model by considering a modification of the classical one. In this modified ASEP model there are two lanes, one for each interface, and the particles can not change a lane. Each particle has an additional property which makes it possible to map it onto the BCSOS2 model. The easiest possible way of doing this is to associate for each particle a number h_i which in BCSOS picture is a height of that lattice site. By this construction BCSOS2 dynamics is achieved by demanding that a particle on the upper lane can move by the normal ASEP dynamics to the right but unnormal to the left, and vice versa on the lower line.

As the models above have a one-to-one mapping at the microscopic level, they also have a mapping in the coarse-grained level as well. The connection is most clear when considering ASEP and BCSOS models [33] such that a particle in ASEP corresponds to an upward step in BCSOS and a hole in a ASEP a downward step. In the hydrodynamic limit the behaviour of the BCSOS interfaces is given by the KPZ equation and that of the ASEP by the Burgers equation. By writing $u(x,t) = -\nabla h(x,t)$ we obtain the Burgers equation from the KPZ equation [34].

3.4 Transport confined by BCSOS interfaces

We consider a single point-sized particle moving between interfaces $h_1(x,t)$ and $h_2(x,t)$ on a lattice (x,y). The lattice point coordinates in the horizontal direction are the same $x = 1, ..., L$ as for the interface model above, again with periodic boundary conditions. In the "vertical" direction, the lattice is infinite and the coordinates are integers $y = ..., -2, 1, 0, 1, 2, ...$ and thus coincide with the possible values of h_1 and h_2 .

We shall denote the location of the particle by (x_p, y_p). The particle does not affect the dynamics of the interfaces but, if needed, a moving interface can push the particle the distance of one or two lattice units in the vertical direction such that the location of the particle also after the change of the interface configuration satisfies the condition

$$h_2(x_p, t) \leq y_p \leq h_1(x_p, t).$$

These are moves of the particle forced by the interface motion. For such moves, we use two "clock updating" schemes for the particle: In scheme (A) the particle is considered in such cases to move together with an interface with its diffusive clock left intact and in (B) its 'clock' is updated after the interface move.

For diffusive moves of the particle, the following two rules are imposed in all cases: First, for a jump $(x_p, y_p) \to (x'_p, y_p)$ to be possible, the product of the interface height differences on the departure site and the arrival site is non-zero: $h_-(x_p, t)h_-(x'_p, t) > 0$ i.e. the channel for the jump between the interfaces must be open at both ends of the jump. Second, an attempted jump arriving outside the region bounded by the interfaces is blocked. In the actual dynamics, the direction of an attempted jump is chosen without any prior knowledge of the ability of the particle to perform the jump.

For diffusion on the square lattice there are a few natural choices for the possible particle jumps $(x_p, y_p) \to (x'_p, y_p)$

1. Dynamics m = 1: The most obvious case are the nearest-neighbor jumps such that the particle jumps in the horizontal direction $(x_p, y_p) \to (x_p \pm 1, y_p)$ (in the vertical direction $(x_p, y_p) \to (x_p, y_p \pm 1)$) with the attempt rate α (with the attempt rate β). To obtain a pure diffusion we set $\alpha = \beta$.
2. Dynamics m = 2: The particle jumps diagonally, i.e. $(x_p, y_p) \to (x_p \pm 1, y_p \pm 1)$ independently, with the attempt rate γ.
3. Dynamics m = 3: This is a combination of the jumps in dynamics 1 and 2.
4. Dynamics m = 4: In this model only the x coordinate of the particle matters and the particle is allowed to perform the jump $(x_p, y_p) \to (x'_p, y_p)$ whenever the channel is open.

For further details see articles III and IV.

The exclusion process follows similar dynamics as the independent random walkers above. The only additional requirement is that two ore more particles cannot be at the same location at the same time. For a pure particle movement this means that an attempted movement is forbidden if the destination site is already occupied. Note that this requirement also induces a particle-interface interaction and thus modifies the dynamics of the interfaces, if interaction in this direction is allowed.

3.5 Simulation methods

In this section a brief overview of the history of the Monte Carlo (MC) method is provided and the theoretical background of MC is discussed.

3.5.1 The Monte Carlo method

The concept of Monte Carlo (MC) methods covers many statistical or stochastic approaches. Consistently if random numbers are used one is doing Monte Carlo. Of course this is a rude generalization, since it would include also SRD [36] and other methods that use a random numbers. In light of the previous statements it is not surprising that one of the fathers of modern physics, Enrico Fermi, developed a statistical algorithm in Rome in early thirties [37], however he did not published it. During the Manhattan Project, Stanislaw Ulam suggested a similar approach to solve certain problems. However the MC method as a name for the statistical approach was first used by Metropolis in 1947 and after that the name endured. More specifically, the method they developed was Markov chain Monte Carlo (MCMC). Therefore it is justified to argue that this was the distinct starting point for the triumphic journey of the MC methods. Indeed any practical MC method requires substantial computational power and it is natural that the starting point of MC is temporally close to the first computer ENIAC [38].

Even though it is almost impossible to know when statistical methods were used for the very first time, it is clear that the first real published MC algorithm was developed in 1953 when Metropolis et al. introduced their method to calculate the equation of the state [39]. The algorithm presented by Metropolis however was only for the case of the Boltzmann distribution. Later on, in 1970, Hastings [40] generalized the algorithm presented by Metropolis et. al in Ref. [39] and laid it onto a mathematically more solid foundation. That time MC methods were used to solve problems in static situations *i.e.* to generate statistically independent samples according to a desired stationary

probability distribution. Furthermore, the original MCMC algorithms required the detailed balance (DB) condition. If one is interested only in stationary quantities only, the DB condition is not mandatory and irreversible algorithms can be used [41].

Since the beginning a variety of different modifications of Monte Carlo methods have accumulated [42, 43, 44], but the attention has been on the computational improvements of the original algorithms [45, 46]. In some cases this computational effectiveness has led to limitations for the usefulness of the algorithm [47]. Another common feature is that algorithms are not versatile expect for a given specific purpose [48].

In the numerical studies presented in this Thesis we use the N-fold algorithm originally presented by Bortz et al. in 1975 [45]. In some cases the algorithm coincides with the one presented by Gillespie [46] a few years later.

3.5.2 Kinetic Monte Carlo methods and their dynamic interpretation

Under the dynamical interpretation the Monte Carlo methods solve the master equation

$$\frac{\partial P(\sigma,t)}{\partial t} = \sum_{\sigma} W(\sigma^{'} \rightarrow \sigma) P(\sigma^{'},t) - \sum_{\sigma^{'}} W(\sigma \rightarrow \sigma^{'}) P(\sigma,t), \tag{3.19}$$

where σ and $\sigma^{'}$ denote different states of the system, $P(\sigma,t)$ is the probability that the system is in state σ at time t and $W(\sigma^{'} \rightarrow \sigma)$ is probability per unit time that the system being in state $\sigma^{'}$ changes its state from $\sigma^{'}$ to σ. For many model systems, the values of W can be parametrized from experiments or microscopic theories. The solution of the Eq. (3.19) is achieved computationally by choosing randomly among various possible transitions to a model system and accepting particular transitions with appropriate probabilities. After each attempted transition time is typically incremented in integral units of MC steps related to some unit time τ.

Static properties of two systems are identical if their Hamiltonians are the same. However dynamical properties are sensitive to the manner in which the time series of events characterizing the evolution of the system is constructed. If the modeling of the real problem is done in a correct way, the MC time corresponds to the real time. Generally if a studied dynamics can be modeled as a Poisson process, the relation between the MC time and real time is on a firm basis.

In some cases the change from the discrete time model to the same model in continuous time model is straightforward [49]. However, in some cases the discrete-time model and its continuous time counterpart produce very different results [50]. In physics this

difference has often been neglected, even though the problem has been encountered often.

3.5.3 The N-fold algorithm

In the N-fold algorithm, which is extensively used in this work, the possible transitions are divided into N classes according to their probabilities. After finding those classes, one finds all lattice points x, which belong to a certain class j. The next step is to calculate the set of time-depended variables

$$Q_i = \sum_{k=1}^{i \leq N} n_{j_k} P_{j_k}, \tag{3.20}$$

where n_{j_k} is number of those lattice points which belong to class j_k and P_{j_k} is the probability associated with j_k. The class j of the event, which will occur, is next determined by finding j such that $Q_{j-1} \leq R < Q_j$, where R is a random number with uniform distribution in the interval $[0, Q_N)$. After finding the class, one has to randomly choose a location (on h_1 or h_2) from this class. By this method the time for something to happen in the lattice is

$$\Delta t = -\frac{1}{Q_N} \cdot \ln(R_1), \tag{3.21}$$

where R_1 is a random number with uniform distribution in the interval $[0, 1)$.

3.5.4 Sampling of quantities

Mean square displacement

The common way to evaluate the tracer diffusion coefficient D_T is to calculate the mean-square displacement (MSD) $\langle \Delta x^2 \rangle$ and then use Eq. (2.2). There are two ways of doing this, either ensemble average (EMSD) or time average (TAMSD). The ergodic hypothesis ensures that for an ergodic system these two averaging procedure produce the same result.

As already stated in Section 2.2.2, for a certain WTD the system is not anymore ergodic and hence those averages are not the same. In fact the temporal averaging can show a diffusive behavior for individual particle even though the behavior of EMSD is sub diffusive, such is shown to occur for example in case where WTD is $\psi(\tau) \sim \tau^{\alpha}$, $\alpha < 1$ [51]. Furthemore ensemble averaging those individual TAMSD

lead to diffusive behavior with normal diffusion coefficient multiplied by $T^{-\alpha}$, where T is the length of trajectory of individual particle. If there are many reasons why the system shows anomalous diffusion the EMSD can not reveal presence of the individual mechanisms leading to anomalous diffusion while the TAMSD can reveal it [52]. The differences of these two averaging procedures become important when information on the transport properties must be gathered from trajectories of only a few particle. This kind of environments and situations are often encountered in biological systems.

Collective diffusion coefficient

In Chapter 2.1.3 we noticed that the collective diffusion coefficient can be determined from the decay of density fluctuations. Even though the equation Eq. (2.10) is spatially Fourier transformed, similar results hold also for sine/cosine transform. Using sine/cosine transform we can write

$$c_k = \sum_{i=1}^{N} \cos(kr_i) \qquad s_k = \sum_{i=1}^{N} \sin(kr_i), \tag{3.22}$$

where r_i is the location of the ith particle, and determine the diffusion coefficient from their decay. We note that an alternative method and a more subtle method to evaluate diffusion coefficients is trough the memory expansion introduced in [53]. The advantage of that is the fast convergence and hence the reduced length and computational cost of the simulation.

4 Results

In order to understand diffusion in an evolving environment one must understand thoroughly the behavior of the environment. This is a common theme of the research reviewed in this Thesis.

4.1 Dynamics of the environment

4.1.1 Properties of ZRP

Usually the way to start to study some unfamiliar system is to monitor its temporal behavior. Since the observation of system as a whole is often impossible one tries to find an order parameter, a single quantity that would characterize the essential features of the dynamics. The principal order parameter of the ZRP is the size of the largest cluster Z_1 and therefore its spatio-temporal behavior is the natural starting point when taking the first look at the actual dynamical behavior. In figure 4.1 a typical behavior of the Z_1 is shown. Clearly there are two distinct regions where the behavior of Z_1 is different, a region with little or no activity at all, or a region with rapid motion of the largest cluster. This kind of burstiness has been documented and studied in a wide range of systems from email patterns [54] to earthquakes [55, 56]. Understanding of this kind of burst processes is based on qualitative arguments. Two mechanisms that lead to the bursty signal have been recognized. One correspond to the fat-tailed interevent distribution $P(\tau)$ observed in email patterns [54] and the other one involves a memory effects like mechanism of earthquakes [55, 56].

In [57] Goh et al. introduced two measures for a bursty signal, a burstiness parameter $B = (\sigma_\tau - m_\tau)/(\sigma_\tau + m_\tau)$, where σ_τ is the standard deviation of the $P(\tau)$ and m_τ its mean, memory $M = n_\tau^{-1} \sum_{i=1}^{n_\tau - 1} (\tau_i - m_1)(\tau_{i+1} - m_2)/(\sigma_1 \sigma_2)$, where n_τ is the number of interevent times measured from the signal and $m_1(m_2)$ and $\sigma_1(\sigma_2)$ are sample means and standard deviations of τ_i's (τ_{i+1}'s) ($i = 1, 2, ..., n_\tau - 1$). The parameter B is a distribution-based measure for the burstiness of the signal and its values are in range $[-1, 1]$, where 1 is for the most bursty and -1 for a regular signal. The memory coefficient M is a correlation-based measure and its range is $(-1, 1)$. It is positive if a short interevent time tends to follow a short one and negative if a short interevent time follows a long one.

For the movement of the largest cluster in ZRP the values of both B and M are almost one for all cases studied. This means that a majority of the observed transitions occurs within a single phase.

In a figure 4.2 the fraction $\tilde{Z}_1 = Z_1/N$ (Eq. 3.6) is presented as a function of density. In all cases the shape of $\tilde{Z}_1(\rho)$ is like a deformed letter S. The shape of the simulated curve is easy to explain heuristically. First, due the discreteness all curves begin at point $Z_1(\rho = 1/L) = 1$. As density increases $\tilde{Z}_1(\rho)$ decreases since the probability that a few particles are at the same location is small and $Z_1 = 1$. This also explain why all curves qualitatively behave similarly for all values of b. $\tilde{Z}_1$ starts to increase at a point where the probability that $Z_1 > 1$ becomes significant. $\tilde{Z}_1$ increases with a non-constant rate to the point after which the rate decreases. We have used this turning point, $\partial^2 Z_1/\partial\rho^2(\rho^*) = 0$ as an estimate for effective "critical" density $\rho_c(L)$. At high densities the theoretical and simulated values correspond to each other very well as they should due to the equivalence of ensembles for the ZRP in the thermodynamic limit.

For $b > 3$ the difference between the effective critical density and its hydrodynamical counterpart decreases like a square root of the system size *i.e.* $\rho_c(L) - \rho_c \sim L^{-1/2}$ (see Fig. 3 of article III). For $b \approx 3$ we do not anymore see this as clear as we did for larger b but the qualitative behavior is similar. For $b \leq 3$ the determination of $\rho_c(L)$ becomes difficult and hence we can not say anything conclusive about its behavior. The finite size analysis of $\rho_c(L)$ is based on Eqs. (3.7) and (3.9).

In figure 4.3 we consider the size of the largest cluster at the moment its relocation, Z_J. The behavior of the ratio Z_J/Z_1 can be understood as follows. At small density the largest cluster is born because suddenly one location gains a few extra particles and shortly loses them. Since the system is very dilute, the difference between largest cluster and the average size on a bulk is at the same order than those extra particles. As the density increases the average size in the bulk increases while the size of condensate does not grow as rapidly and hence the decrease of the ratio. Deep in the condensed phase only two lattice sites are participating in this reallocation of the mass and hence the fraction $\langle Z_J\rangle/\langle Z_1\rangle \approx 1/2$. Near the dip, which is nearby and scales in a similar way as $\rho_c(L, b)$, the system is in a crossover region were both of these mechanisms are present.

In understanding diffusion processes occurring in the system the characteristic timescales of the condensate are in a crucial role. From Fig. 4.4 we see that in the fluid phase, *i.e.* when the density is below $\rho_c(L)$, the lifetime distribution of the condensate is exponential. As the density approaches $\rho_c(L)$ an extra hump emerges in the lifetime distributions. This is a clear signal that a macroscopic condensate stays at one specific location over a long period of time before reallocation. The fact that $\langle Z_J\rangle/\langle Z_1\rangle \approx 1/2$, verifies the results for the expected lifetimes for a condensate in a condensed phase

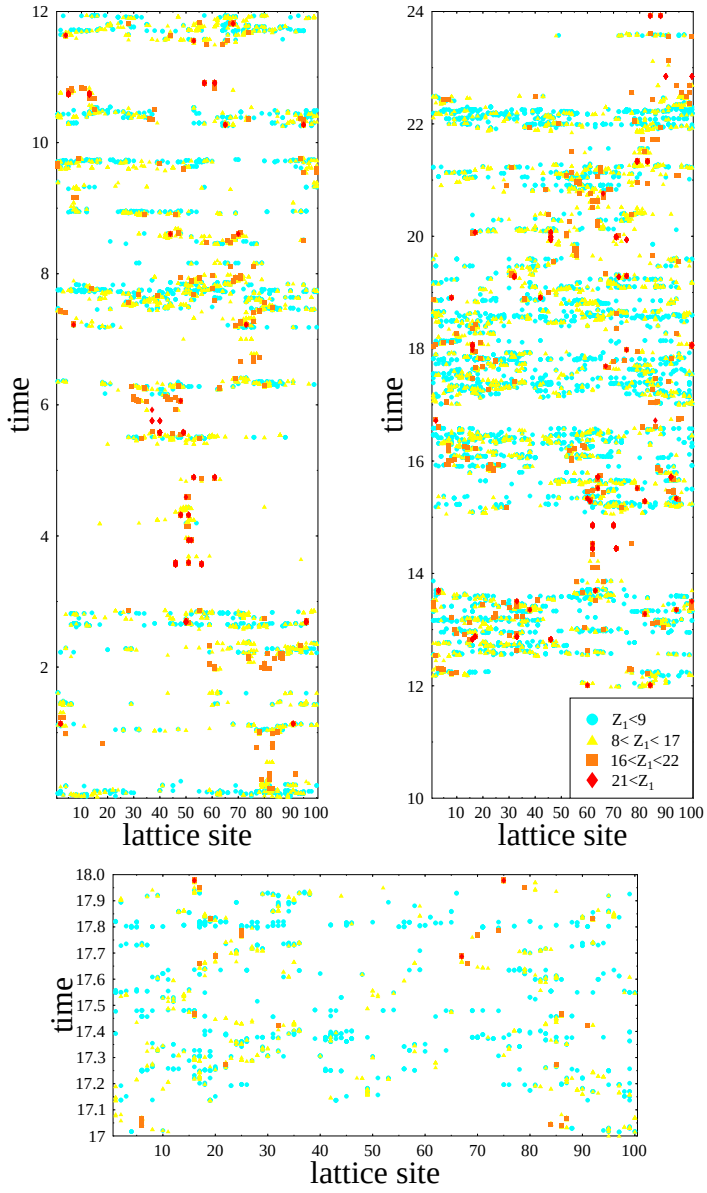

Figure 4.1: The location of the largest cluster as a function of time for $b = 5$, $\rho = 3/4$ and $L = 100$. Each symbol marks the position of the largest cluster just after a jump and also indicates the size of the cluster at that moment. In the lower panel we show a magnification, from just below the middle of the upper right panel. The time axis has been scaled by a factor 10^5.

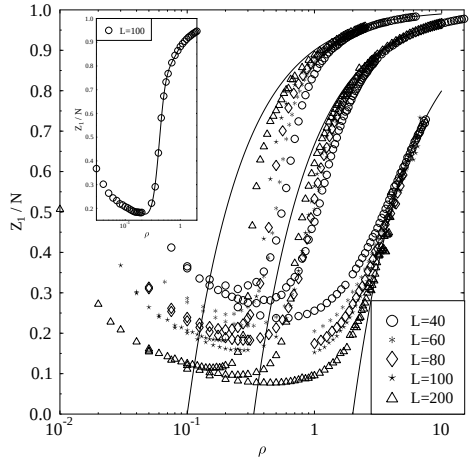

Figure 4.2: The size of the largest cluster as a function of the density for $b = 2.5, 5, 12$ (from bottom to top). The symbols denote the Monte Carlo data and the full curves show the behavior at the thermodynamic limit according to Eq. (3.6). In the inset, we show a typical fit, here for $b = 12$ and $L = 100$, from which $\rho_c(L)$ is found at the turning point of the fitted function.

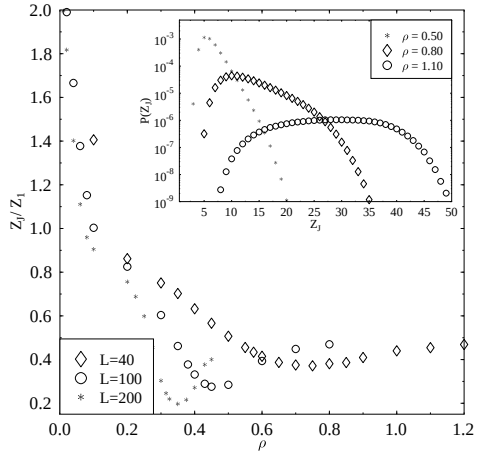

Figure 4.3: The average size of the largest cluster at the moment of relocation for $b = 12$. The inset shows the distribution of Z_J for $b = 5$ and $L = 100$ with the density smaller than, equal to, and greater than $\rho_c(L) \approx 0.8$.

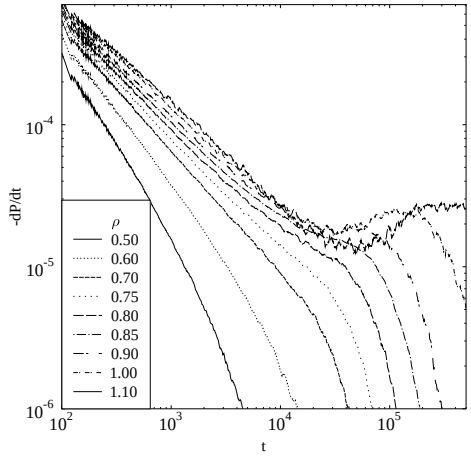

Figure 4.4: The distribution of lifetimes of the largest cluster for $b = 5$ and $L = 100$ at various densities. For the case shown $\rho_c(L) \approx 0.8$.

presented by Godreche et al. in Ref. [58]. From Fig. 4.3 we can see that this assumption is valid only deep in the condensed phase when the system is in a pure condensed phase with no coexisting fluid phase.

4.1.2 Properties of the BCSOS2 model

According to Sec. 3.3 the roughness exponent for the interfaces in the BCSOS model is $\alpha = 1/2$. As one can see from figure 4.5, for a small system size also the roughness of the difference process obeys this power law up to some critical system size where its value saturates.

In Fig. 4.6 we show the behavior of the stationary width W_1^s scaled by $L^{-1/2}$ for interfaces driven symmetrically against each other. The roughness dip is a finite size effect. Phenomenologically the reason for the dip is reduction of the available configuration space, when interfaces meet each other. Naturally the number of blocked configurations increases as the system size increases and therefore as $L \to \infty$ there is discontinuity in the roughness for $f \to 0$. This reduction of the parameter space is also present in other quantities describing the distribution of the interfaces. It turns out that the skewness of the distribution start to deviate from the zero at the point were the dip occurs and also the expected kink density shows this dip near by the value f_w, see figure 4.7. This kind of non-monotonicity has been experimentally observed

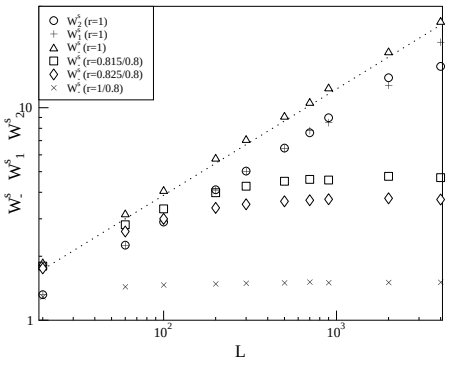

Figure 4.5: The size dependence of the stationary widths for a propagating pair of interfaces h_1 and h_2 and their difference h_- for a few values of the parameter r. The slope of the dotted line corresponds to the value of the roughness exponent $\beta = 1/2$

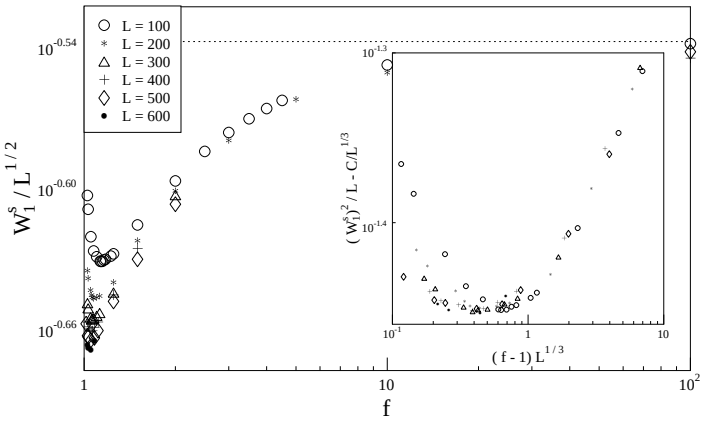

Figure 4.6: The stationary width W_1^s scaled by $L^{-1/2}$ for interfaces driven symmetrically against each other as a function of the parameter f. The dashed line indicates the stationary width of an isolated interface. The inset shows the scaling of the location of the dip bottom.

prior to our simulation in Ref. [59] concerning domain walls in magnets. In figure 4.7 we also show the stationary state bubble size distribution, which controls diffusion between the interfaces as studied next.

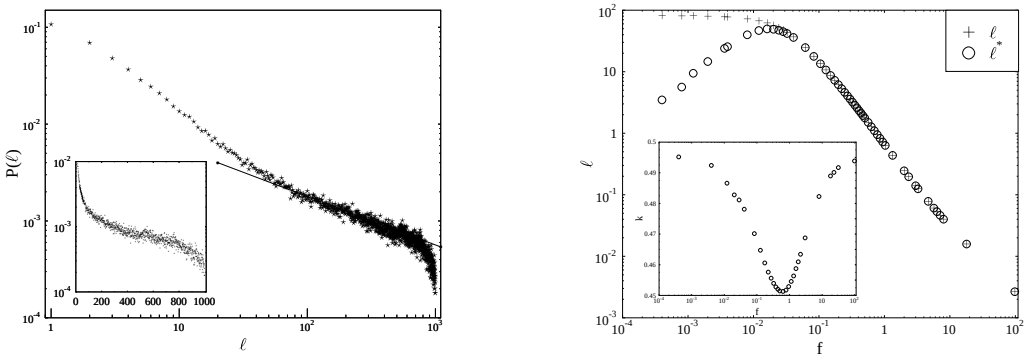

Figure 4.7: In the figure on the left we show the bubble size distributions. In the figure on the right we show the average bubble size $\bar{l}$ and kink density $\bar{k}$ as a function of f is presented . We show the bubble size normalized in two ways: using the real l where bubble sizes $0 \leq l \ll L$ and $\bar{l}^*$ where $0 \leq l \leq L$ are taken into account

4.2 Results for diffusion

4.2.1 Diffusion in ZRP

In Fig. 4.8 the collective diffusion coefficient D_C determined by Eq. (3.22) as well as the center of mass diffusion coefficient D_{CM} from the center-of-mass movement is presented. It is found that $D_C > D_{CM}$ for $\rho < \rho_c(L)$, $D_C \approx D_{CM}$ at $\rho = \rho_c(L)$ and $D_C < D_{CM}$ for $\rho > \rho_c(L)$. The reason why D_{CM} is bigger than D_C for large ρ is related to the dynamics of the condensate, namely D_{CM} can increase even though the condensate stays as the biggest cluster due the transport of individual particles across the system. The fact that $D_C \approx D_{CM}$ around $\rho = \rho_c(L)$, indicates again that $\rho_c(L)$ is a relevant effective density since apparently it is the point where the rate of mass transport slows down rapidly.

Let us continue by considering collective diffusion and center of mass diffusion in the framework provided by the theory of CTRW presented in Chapter 2.2. Clearly, there are several fundamental differences between these two processes. One major difference is the lack of direct association of collective diffusion with the movement of any well

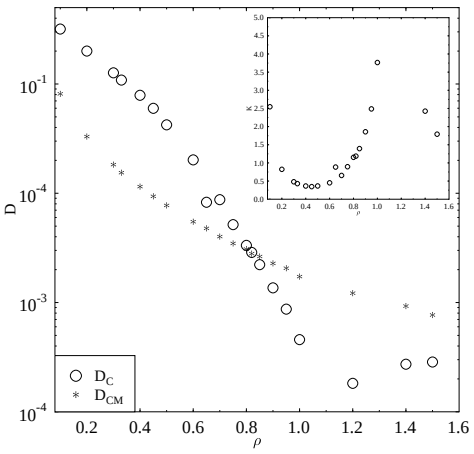

Figure 4.8: The diffusion coefficients D_C and D_{CM} and the compressibility $K(\rho)$ for $b = 5$ and $L = 100$.

defined collection of mass in the entire density range. In the condensed phase we can associate, quite reasonable, collective diffusion with the movement of largest cluster. Therefore the waiting time distribution for collective diffusion can be approximated by the waiting time distribution for the largest cluster presented in Fig. 4.4. Although we can not determine the actual direction to which the largest cluster moved during its relocation process, it is justifiable to argue that there are (temporarily) preferred directions in the system.

For collective diffusion the jump length distribution below $\rho_c(L)$ is highly peaked at one and elsewhere it is a constant. This peak starts to decrease as the density increases and in the condensed phase the jump lengths are uniformly distributed. Hence the variance of the jump length distribution is always bigger than one and increases as for increasing density until it saturates to the value corresponding to the variance of an uniform distribution. The expected jump length is presented in figure 7 of article III. For the center of mass movement every jump is due to an exchange of one particle and hence its variance is always exactly one. For the center of mass motion the waiting time distribution is an average of Eq. (3.21) over the process.

Since we consider a canonical system with fixed density the average waiting time for the center-of-mass motion is always much smaller than that for collective diffusion. In fact it is of the order of one while for colletive motion it can be effectively infinite even in a canonical system. Combining the notions above of the expected waiting times and the variace of the jump lengths, the CTRW picture of Section 2.2.2 qualitatively agrees

with the result presented in Fig. 4.8. The compressability K, which is proportional to particle number fluctuations, is expected to diverge at the point of phase separation. In Fig. 4.8 no such divergence observed aroun $\rho_c(L)$, but the value of K starts to increase rapidly there. With the available computational resources the study of a possible finite-size or finite-time effect was not feasible. In the case of anomalous fluctuations the interpretation of K is expected to change.

Tracer diffusion in a two species ZRP

As an extension of the work published in article II, we have considered also tracer diffusion in a two species ZRP where the environment, *i.e.* particles of species A, obeys Evans type dynamics with $b = 12$ and the jump rate of the tracer particle (B) is determined from the environment entirely also by Evans form of dynamics with different parametrization. Below we show some results that shed light on the mechanism through which condensation influences diffusion. To this end, we considered situations where both of the free parameters, b and u_0 can vary. Since the dynamics of the environment also here is independent of that of the diffusing particle, the environment behaves as discussed in Section 4.1.1. The simulations we performed for both clock updating schemes defined in Chapter 3.4. In ZRP there are no transition forced by the environment since there are no spatial restrictions on particle motion. In ZRP, the clock updating scheme determines what happens to the jump rate of the tracer particle when the environment changes at the location of the particle.

In Fig. 4.9 we show the tracer diffusion coefficient D_T for the species B. Due to the form of the Evans interaction, the choice of b for the tracer particle does not have a strong effect, when only the environment provided by the particles of type A contribute to its rate. However, the ratio of the prefactors u_0 for particles of type A and B controls the effect of particle number fluctuations on lattice site on the realized jump rates. A very fast B particle spends most of the time in the bulk, not in the site containing the largest cluster. In that limit the clock updating scheme has no effect on D_T and, overall, it only has no major effect on its dependence on ρ for fixed b. In the case considered in Fig. 4.9 the value $\rho \approx 1/3$ is the one for which the size of the largest cluster begins to increase rapidly, *i.e.* somewhat below the crossover $\rho_c(L)$. Around that point larger clusters capable of changing the effective jump rate of the tracer particle begin to emerge. The saturation of D_T to a level determined by the value of u_0 observed well above $\rho_c(L)$ is related to the time scale used in determining the MSD as compared to the time scale of the condensate, even if the MSD corresponds to the system size. The tracer particle actually probes the fluctuation time scale of the condensate rather than its relocation time scale.

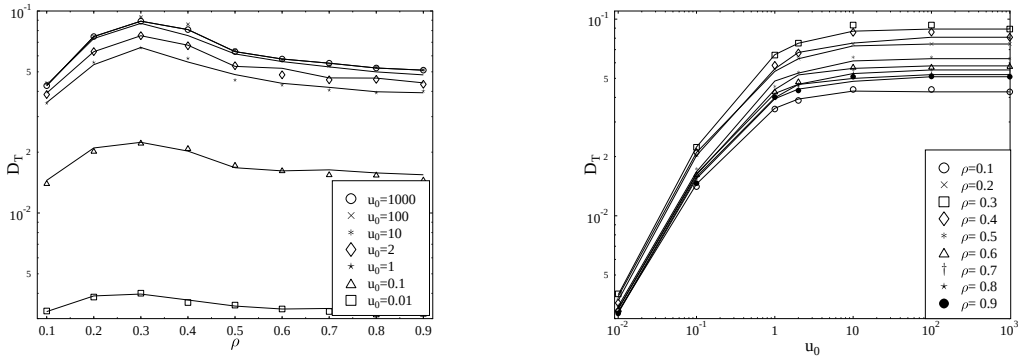

Figure 4.9: In the figure on the left we show simulation results for tracer diffusion coefficient D_T as a function of the density of the environment. For the environment and the tracer particle $b = 12$ and u_0 for the tracer particle was varied. The system size is $L = 100$. In the figure on the right we show simulation results for the tracer diffusion coefficient D_T as a function of u_0 (in units where u_0 for the background is one).

4.2.2 Transport confined by interfaces

Diffusion between evolving interface

The most important factor controlling diffusion between the interfaces is the dynamics of the bubbles. In the case of slow diffusion the question is: Is the bubble open at the location of the particle at the specific moment of time? In other words, if the particle belongs to a bubble greater than two it can perform a jump and hence the diffusion coefficient is

$$D_t(f, \mu) = g(f) D^m_{free}(\mu) \tag{4.1}$$

where $g(f)$ is the probability that the particle can perform a jump inside the bubble. As can be seen from figure 4.10 this mean-field prediction works very well for $\mu < 1$. Scaling f by

$$\sigma(\mu) = \sqrt{1 + \mu} \tag{4.2}$$

we obtain the data collapse presented in the inset of figure 4.10. This scaling however works well only below the roughness dip. In the strong drive limit, *i.e.* for $f \to \infty$, the question is: Does the particle make the jump fast enough. Therefore we rescale the observed diffusion coefficient as

$$D_t(f, \mu) = D^m_{obs}(\mu)/(1 - \exp(-\mu\tau_2)), \tag{4.3}$$

where $\tau_2 \approx 1/2$ is the lifetime of a bubble of size $\ell = 2$. These two scaling scenarios, *i.e.* Eqs. (4.2) and (4.3), are incompatible because the rate limiting mechanisms are different. For fast particle jumps, an adiabatic approximation, within which diffusion is dominated by the bubble dynamics, is also shown in the figure. In the adiabatic approximation the diffusion coefficient is

$$D_{adia}(\mu, f) = \frac{1}{2}\frac{1}{T_{mob}}B(f)^2, \tag{4.4}$$

where T_{mob} is the time scale of bubble motion abd $B(f)^2$ is the mean-square displacement (per jump) of the bubble obtained as $B^2 = \langle |b_{new} - b_{old}| \rangle$. Here b_{new} and b_{old} are the locations of a bubble before and after the change in the bubble size.

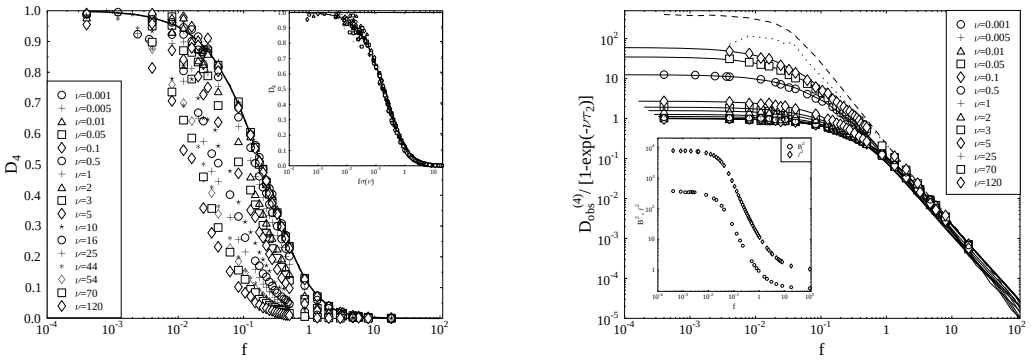

Figure 4.10: In the figure on the left we show simulation results (plotting symbols) for $D_4(\mu, f)$ and the mean-field prediction for the small μ limit (solid line). In the inset we show the data collapse discussed in text. In the figure on the right we show a data collapse for the large f behavior of D_{obs} by using the scaling form of Eq. (4.3). The plotting symbols show the simulation results and the solid lines give the mean-field approximation for small μ of Eq. (4.1) with f scaled by the factor $\sigma(\mu)$ given in Eq. (4.2). The dashed line is the adiabatic approximation of Eq. (4.4) and the dotted line is the finite-size-corrected infinite-rate approximation described in text. In the inset we show the comparison of the behavior of the jump-length factor B^2 and the mean squared bubble size ℓ^2 .

In figure 4.11 we consider modifications to this behavior by allowing two-dimensional jumps and, on the other hand, by changing the clock updating scheme. A similar mean-field approximation as the one presented for the dynamics $m = 4$ above is harder do to for the dynamics $m = 1 - 3$ (see Section 3.4), since two dimensional diffusion depends not only on the horizontal size of the bubbles, but it depends also on the actual shape of the bubble, but nevertheless the main features of diffusion remain the same apart from the case of weak drive. The effect of the clock updating

scheme is much more dramatic in the region, where the waiting times for interface motion and particle jumps coincide, resulting in a phase-transition like signal in D_T even if its origin is purely kinetic.

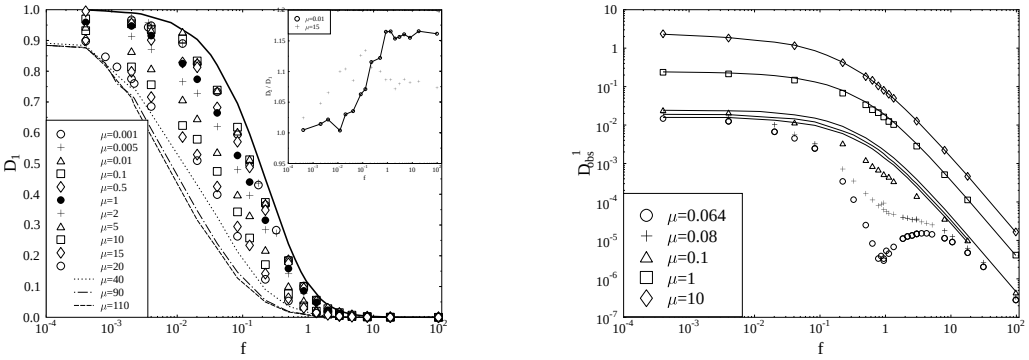

Figure 4.11: In the figure on the left we show diffusion coefficient D_1 for the particle clock updating scheme A. For comparison we show also by the full line the mean-field approximation, c.f. Fig. 5. In the inset we show the ratio $D_2(\mu/2)/D_1(\mu)$. In right figure the diffusion coefficient D_1 for the particle clock updating scheme B is shown. The full curves show the corresponding data for scheme A.

Two dimensional exclusion process in a rough channel

In figure 4.12 we show snapshots of the scaled occupation probability. The spatial inhomogeneity decreases for increasing β, which is the rate of diffusion in the vertical direction. With flat walls, spatial homogeneity is achieved in the simulation for all values of $\beta > 0$, while for increasing roughness the value of β required for approximate homogeneity is larger. Homogeneity gets broken because the particles tends to drift towards the wall at locations with long slopes. Spatial homogeneity becomes important when considering the current through the system. For spatially homogeneous density the mean-field prediction $I(\rho) = \alpha\rho(1-\rho)d$ for the averaged current works well, and increasing deviations are observed for increasing the wall roughness. The amount of this deviation decreases for increasing β.

In Fig. 4.13 we show the expected value of the particle current I crossing a lattice site as a function of the wall roughness W defined by Eq. 3.18. The value of the current for a given wall roughness depends strongly also on other properties of the walls. Configurations corresponding to the extrema of the current we created by running variations of usual BCSOS dynamics for a while starting from certain initial configurations, a disordered one, a flat one and a faceted one. For example, the smallest currents were

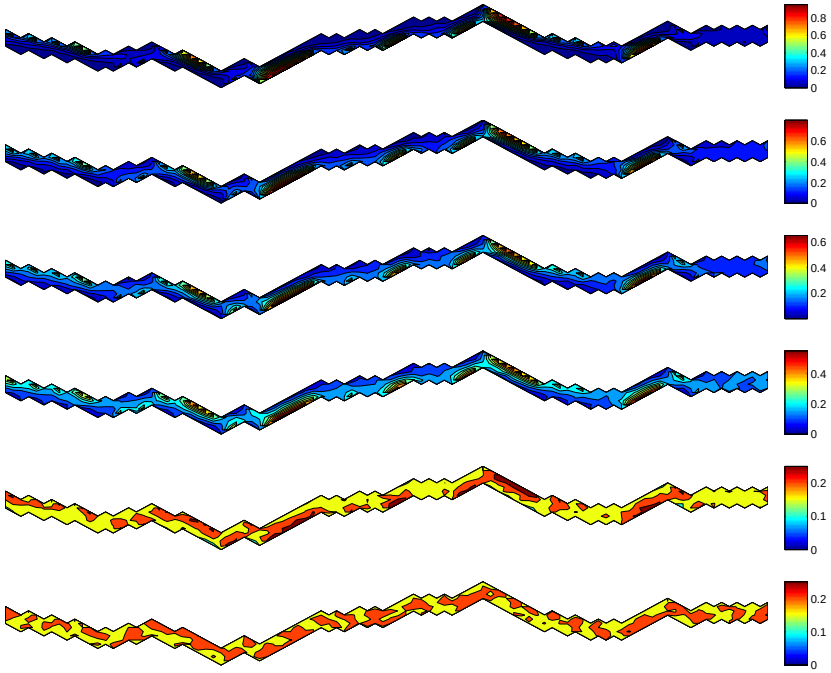

Figure 4.12: Probability to find particle at location (i, j) with several parameter β values. Here the red color indicates highest densities and blue color lowest densities. The average density is $\rho = 0.2$ and the drift $\alpha = 1$. The system size is $L = 100$ and the widh of the channel four lattice units. The parameter β controlling diffusion in the vertical direction increases from top to bottom from 0.25 to 20.

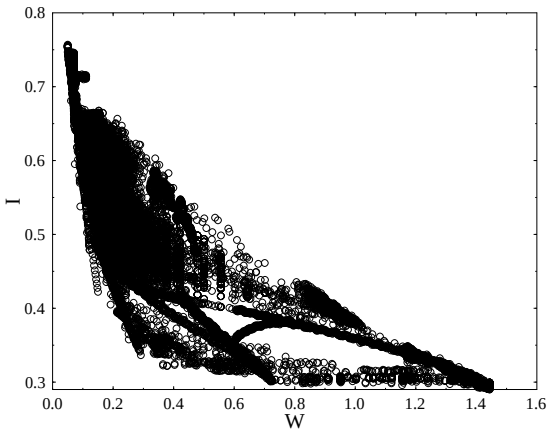

Figure 4.13: Averaged current over cross-section measure at $x = L$ as a function of roughness of the wall. System size is $L = 100$, $\alpha = 1$, $\beta = 0.5$ and $\rho = 0.25$.

obtained by generating the interface configurations by 'depositing 'particles' anywhere on the interface such that they slide down to the closest interface height minumum. The maximum current for a given roughness was obtained by producing interfaces such that the BCSOS dynamics corresponds to one-dimensional ASEP, where in the ASEP interpretation particle a randomly chosen hops to a location as far as possible from the closest particles with conserving the order of particles in the system. This way it was possible to achieve interface configurations with very different topography and effectively scan the available phase space for wall configurations.

5 Discussion

In this Thesis particle transport in evolving and restricted environments was investigated by Monte Carlo simulations. In all models considered in this Thesis strong finite-size or crossover effects are present. In addition to finite-size effects, we considered the dependence of diffusion on the "microscopic" details of the interaction of the diffusing particle and its environment. The main question arising is the influence of an environmental change on the particle waiting time distribution. If the changes in the environment do not cause any changes in the WTD of the particle, the particle acquires a memory in sense that it remembers how long it has been waiting. Physically it would be possible e.g. if the particle gains some extra energy from the surroundings. If the WTD is strongly influenced by the interaction with the dynamic environment, anomalous diffusion may be observed, which is a subject of further studies.

In all cases considered the dynamics of the environment has a dominant role from the point of view of diffusion and, hence, in many cases the behavior of the diffusion coefficient of a single particle is obtained entirely from the dynamics of the environment. Diffusion between interfaces driven towards each other was found to depend entirely on the dynamics of the bubbles and the results are assumed to be generalizable to many other systems with dynamic restricting geometry. Even though the motion of particles was always diffusive, it is not entirely impossible that with certain free particle rates the bubble dynamics could lead anomalous diffusion due to the fact that the lifetime distribution of the bubbles displays a power law behavior.

The particle current for two-dimensional ASEP in a rough channel was found to depend strongly on the configurations of the channel walls. Conventionally used characteristic quantities were found to be inadequate in describing the current in the channel. As a conclusion the channel profile has a much greater impact on the particle flow and its dispersion than it has for laminar Navier-Stokes flows considered in the literature.

Furthemore, some stationary and dynamical properties of the environment can sometimes be probed by studying the behavior of transport more easily than from a direct observation of the environment dynamics itself. One reason for that is the fact that the diffusion coefficient is a product of temporal and spatial factors c.f. Section 2.2, hence providing a spatio-temporal overview of the system. However, in some cases the chosen microscopic interaction between the environment and the diffusing particles may hinder the separation of these effects.

When determining the collective diffusion coefficient it should be calculated in the limit of long times. When calculating collective diffusion in a condensed phase of ZRP the determination of the actual limit after which we could be sure that we are in a proper timescales was difficult. This is due the time scale separation between the characteristic timescale of particles and the lifetime of the largest cluster.

A natural and logigal way to continue research on this path is to include theflow-environment interactions in both directions. This interaction is naturally present in an exclusion process. To proceed futher requires a study of the effect of the dynamical environment in a realistic flow at systems so small that the Navier-Stokes or other continuum descriptions fail to describe the dynamics, physical applications being in nanofluidics.

6 Appendix

6.1 More detailled derivation of CTRW

We use the recursion relation approach to solve the general CTRW on a lattice. The notations obey the notations of Ref. [20].

For simplicity let us assume that the particle has performed its latest transition at time $t = 0$. Then $\psi_{n,m}(t)$ is the probability density that the particle jump at time t from site m to site n after waiting time t on m, it must be positive semidefinite and it must be normalized when integrated over infinity *i.e.*

$$\sum_n \int_0^\infty dt' \psi_{n,m}(t') = 1. \tag{6.1}$$

Since, the tracer diffusion coefficient is usually obtained by the mean-square displacement via Eq. (2.2) then understanding of tracer diffusion is reduced to the understanding of the probability distribution function of the location of the particle at time $t > 0$ with the condition that $t = 0$ it was in a given lattice site l *i.e* the conditional probability $P(n, t|l, 0)$.

Let $Q_\nu(n, t)$ be the probability density that the particle has performed its νth transition at time t and reached site n. Recursively this can be write as

$$Q_\nu(n, t) = \sum_m \int_0^t dt' \psi_{n,m}(t - t') Q_{\nu-1}(m, t'). \tag{6.2}$$

This relation however is valid only for $\nu \geq 2$ since the first transition has to be treated differently,

$$Q_1(n, t) = \sum_m h_{n,m} P(m, t = 0), \tag{6.3}$$

where $h_{n,m}$ is the WTD for the first transition from m to n. By summing over ν i.e, the numbers of transitions in which the particle has moved to n we obtain the probability density that site n is occupied by a transition at time t

$$Q(n, t) = \sum_\nu Q_\nu(n, t). \tag{6.4}$$

This equation can of course be written for all lattice sites, not only for n. Now we can write an equation for $Q(n,t)$ similar to Eq. (2.11) for $Q_\nu(n,t)$. Now the probability density in Eq. (2.12) becomes

$$Q(n,t) = \sum_m \int_0^t dt' \psi_{n,m}(t-t') Q(m,t'). \tag{6.5}$$

By performing a spatial Fourier and temporal Laplace transfomation we obtain

$$\tilde{Q}(k,s) = \frac{\tilde{h}(k,s) P(k,t=0)}{1-\tilde{\psi}(k,s)}. \tag{6.6}$$

Now we have obtain the probability that the particle has just arrived in site n at time t'. The probability $P(n,t|l,0)$ is thus related to $P(n,t')$. If the particle arrived to site n at t', then the probability that it still is in the same site depends of the probability that no further jumps occur between t' and t. If no transitions occured at all, the particle was already in site n at time $t=0$. Finally we obtain the required probability

$$P(n,t|l,t=0) = \int_0^t dt' \Psi(t-t') Q(n,t') + H(t) P(n,t=0), \tag{6.7}$$

where $\Psi(t-t')$ is probability that no jump occure between times t' and t and $H(t)$ is the probaility that no jumps occured at all i.e.,

$$\Psi(t) = 1 - \sum_n \int_0^t dt' \psi_{n,m}(t') \quad \text{and} \quad H(t) = 1 - \sum_n \int_0^t dt' h_{n,m}(t'). \tag{6.8}$$

By Laplace and Fourier transforms we get the result:

$$\tilde{P}(k,s) = \frac{1 - \tilde{h}(0,s) + \tilde{h}(k,s) - \tilde{\psi}(k,s) + \tilde{h}(0,s)\tilde{\psi}(k,s) - \tilde{h}(k,s)\tilde{\psi}(0,s)}{s(1-\tilde{\psi}(k,s))}, \tag{6.9}$$

which simplifies for a separable CTRW to

$$\tilde{P}(k,s) = \frac{1 - \tilde{h}(0,s) + \lambda(k)[\tilde{h}(s) - \tilde{\phi}(s)]}{s(1-\lambda(\tilde{k})\phi(\tilde{s}))}. \tag{6.10}$$

If we consider a stationary ensemble the waiting time distribution for the first jump is

$$h_{n,m}(t) = \frac{\int_0^\infty dt' \psi_{n,m}(t+t')}{\sum_n \int_0^\infty dt \int_0^\infty dt' \psi_{n,m}(t+t')}, \tag{6.11}$$

for which the Fourier-Laplace transform is

$$\tilde{h}(k,s) = \frac{\tilde{\psi}(k,0) - \tilde{\psi}(k,s)}{\bar{t}s}, \tag{6.12}$$

where

$$\bar{t} = \sum_n \int_0^\infty dt' t' \psi_{n,m}(t'). \tag{6.13}$$

Finally we obtain the conditional probability in a stationary ensemble

$$\tilde{P}(k,s) = \frac{1}{s} + \frac{1}{\bar{t}s^2} \frac{[1-\tilde{\psi}(0,s)][\tilde{\psi}(k,0)-1]}{1-\tilde{\psi}(k,s)}. \tag{6.14}$$

The result above is for coupled case. For decoupled case

$$\tilde{P}(k,s) = \frac{1}{s} + \frac{1}{\bar{t}s^2} \frac{[1-\tilde{\phi}(s)][\lambda(\tilde{k})-1]}{1-\lambda(\tilde{k})\tilde{\phi}(s)}. \tag{6.15}$$

6.2 Fourier and Laplace transformations

The Lablace transformation is defined as

$$P(\tilde{k},s) = \int_0^\infty dt \exp(-st) P(k,t) \tag{6.16}$$

and discrete Fourier tranform as

$$F_k = \sum_{n=0}^{N} f_n \exp(-ink), \quad n = 1, ..., N. \tag{6.17}$$

For both trasformations the transformations of convolutions

$$(f * g)(t) = \int_{-\infty}^{-\infty} f(t-\tau) g(\tau) d\tau$$

becomes a product of individual transformations i.e $L((f*g)(t)) = L(f)L(g)$, where L is either Lablace or Fourier transformation.

6.3 Probabilities

If $h(t) = \psi(t)$ the probability that n event occurs in time t is

$$P(n|t) = F^{n*}(t) - F^{(n+1)*}(t),$$

where F^{n*} is n-fold convolution of F with itself. For F^{n*} we get following proberties

$$F^{1*} = F, \qquad F^{(i+1)*} = F^{i*} * F.$$

Furthemore if F has a density ψ then F^{i*} has the density $\prod_{l=1}^{i} \psi$. [60]

So the expected number of event in time t is

$$\langle n(t) \rangle = \sum_{n=0}^{\infty} nP(n,t) = \sum_{n=0}^{\infty} n[F^{n*}(t) - F^{(n+1)*}(t)] = \sum_{n=1}^{\infty} F^{n*}(t)$$

which Laplace transformation is

$$\langle n(s) \rangle = \sum_{n=1}^{\infty} \int_0^{\infty} F^{n*}(t) e^{-st} dt = \sum_{n=1}^{\infty} \frac{1}{s} \psi(s)^n = \frac{\psi(s)}{s(1-\psi(s))}.$$

Similarly we find that

$$\langle n(s)(n(s)-1) \rangle = \frac{2\psi(s)^2}{s(1-\psi(s))^2}$$

If $h(t) \neq \psi(t)$ we get

$$P(n|t) = H(t) * F^{(n-1)*}(t) - H(t) * F^{n*}(t) = H(t) * (F^{(n-1)*}(t) - F^{n*}(t)).$$

so the expected number of event in time t is

$$\langle n(t) \rangle = \sum_{n=0}^{\infty} nP(n,t) = \sum_{n=0}^{\infty} H(t) * [nF^{(n-1)*}(t) - nF^{n*}(t)] = H(t) * \sum_{n=0}^{\infty} F^{n*}(t),$$

which Laplace is

$$\langle n(s) \rangle = \Big(\int_0^{\infty} H(t) e^{-st} dt \Big) \Big(\sum_{n=1}^{\infty} \int_0^{\infty} F^{n*}(t) e^{-st} dt \Big) = \sum_{n=0}^{\infty} \frac{1}{s} \psi(s)^n = \frac{1-\psi(s)}{s\bar{t}} \frac{1}{s(1-\psi(s))} = \frac{1}{\bar{t}s^2}$$

and

$$\langle n(n-1)(s) \rangle = \frac{2\psi(s)}{(1-\psi(s))\bar{t}s^2}$$

In order to get the final result we must find expression to $h_{n,m}(t)$. Feller derive expression for $h(t) = (1 - \int_0^t \psi(\tau) d\tau) \bar{t}^{-1}$ considering ongoing renewal process [60]. In [61] Lax et. all however provide more clear derivation throw conditional propabilities:

$$\phi(\tau) = \int_{\tau}^{\infty} \psi(t) dt = 1 - \int_0^{\tau} \psi(t) dt = 1 - \Psi(\tau). \tag{6.18}$$

Probability that transition occur at time t when it has already waited time τ is

$$\psi(t|\tau) = \frac{\psi(t+\tau)}{\phi(\tau)}. \tag{6.19}$$

and thus the waiting time for the first jump is

$$h(t) = \frac{\int_0^\infty \psi(t|\tau)\phi(\tau)d\tau}{\int_0^\infty \phi(\tau)d\tau}. \tag{6.20}$$

Since $\bar{t} = \int_0^\infty [1 - F(t)]dt$

$$h(t) = \frac{\int_0^\infty \psi(t+\tau)d\tau}{\bar{t}}. \tag{6.21}$$

Let change variable$\tau = x - t$,$d\tau = dx$

$$h(t) = \frac{\int_t^\infty \psi(x)dx}{\bar{t}} = \frac{1 - \int_0^t \psi(x)dx}{\bar{t}} = \frac{1 - \Psi(t)}{\bar{t}}. \tag{6.22}$$

$$\int_0^\infty h(t)dt = \frac{\int_0^\infty [1 - \Psi(t)]dt}{\bar{t}} = 1$$

This means that $h(t)$ is propability density eventhought the expected value $\bar{t}$ do not exist.

References

[1] V. Privman. *Finite Size Scaling and Numerical Simulation of statistical Systems.* Wordl Scientific Publishing Co. Pte. Ltd, 1990.

[2] S. Chandrasekhar. Stochastic problems in physics and astronomy. *Modern Physics*, 15(1), 1943.

[3] W Montroll Elliott. and Weiss George H. Random walks on lattices ii. *J. Math. Phys.*, 6(2), 1965.

[4] F. Solomon. *Ann. Prob.*, 3(1), 1975.

[5] H. Kesten, M. V. Kozlov, and F. Spitzer. *Compositio Math.*, 33(145), 1975.

[6] Ofer Zeitouni. Random walks in random environments. *J. Phys. A: Math. Gen.*, 39:R433–R464, 2006.

[7] S. Alexander, J. Bernasconi, W. R. Schneider, and R. Orbach. Excitation dynamics in random one-dimensional systems. *Reviews of Modern Physics*, 53(2), 1981.

[8] Pierre Le Doussal, Cecile Monthus, and Daniel S. Fisher. Random walkers in one-dimensional random environments: Exact renormalization group analysis. *Phys. Rev. E*, 59(5), 1999.

[9] Ya. G. Sinai. *Theory of Prob. and Appl.*, 27(2)(247), 1982.

[10] P. Sekhar Burada, Peter Hänggi, and Fabio Marchesoni. Diffusion in confined geometries. *arXiv:0808.2345*, 2008.

[11] B. Mehlig, M. Wilkinson, V. Bezuglyy, K. Gustavsson, and K. Nakamura. Multiple regimes of diffusion. *Phys.Rev.E.*, 80(011139), 2009.

[12] C. Chevalier and F. Debbasch. Lateral diffusions: The influence of geometry fluctuations. *EPL*, 89(38001), 2010.

[13] A. Einstein. Über die von der molekularkinetischen theorie der wärme geforderte bewegung von in ruhenden flüssigkeiten suspendierten teilchen. *Annalen der Physik*, 322(8):549–560, 1905.

[14] A. Einstein and R. Furth. "on the movement of small particles suspended in a stationary liquid demanded by the molecular-kinetic theory of heat, 1926.

[15] Karl Pearson. The problem of the random walk. *Nature*, 72:294, 1905.

[16] Ralf Metzler and Joseph Klafter. The random walk's guide to anomalous diffusion: A fractional dynamics approach. *Phys. Rep.*, 339, 2000.

[17] J.-P. Hansen and I.R. McDonald. *Theory of Simple liquids*. Elsevier, 2 edition, 1986.

[18] P. M. Chaikin and T. C. Lubensky. *Principles of Condensed Matter Physics*. Cambridge University Press, 1995.

[19] Mark Kac. Random walk and the theory of brownian motion. *The American mathematical Monthly*, 54(7):369–391, 1947.

[20] J.W. Haus and K.W. Kehr. Diffusion in regular and disordered lattices. *Phys. Rep.*, 150(5&6), 1987.

[21] J. Klafter, A. Blumen, and M. F. Shlesinger. Stochastic pathway to anomalous diffusion. *Phys. Rev. A.*, 35(7):3081, 1987.

[22] Alberto Saa and Roberto Venegeroles. Ergodig transitions in continuos-time random walks. *Phys. Rev. E.*, 82:031110, 2010.

[23] G. Bel and E. Barkai. Weak ergodicity breaking in the continuous-time random walk. *Phys. Rev. Lett.*, 94(240602), 2005.

[24] Miguel Montero and Jaume Masoliver. Random time-scale invariant diffusioin and transport coefficient. *Phys. Rev. E*, 78:061115, 2007.

[25] Vincent Tejedor and Ralf Metzler. Anomalous diffusion in correlated continuous time random walks. *J. Phys. A: Math. Theor.*, 43:082002, 2010.

[26] F. Spitzer. Interaction of markov processes. *Adv. Math.*, 5:246–290, 1970.

[27] M. R. Evans, S. N. Majumdar, and R. K. P. Zia. Canonical analysis of condensation in factorised steady state. *J. Stat. Phys*, 123:357, 2006.

[28] M. R. Evans and S. N. Majumdar. Condensation and extreme value statistics. *J. Stat. Mech.*, page P05004, 2008.

[29] M. R. Evans, S. N. Majumdar, and R. K. P. Zia. Factorised steady states in mass transport models. *J. Phys. A: Math. Gen.*, 37:L275, 2004.

[30] M. R. Evans and T. Hanney. Phase transition in two species zero-range process. *J. Phys. A: Math. Gen.*, 36(28):L441–L447, 2003.

[31] M. R. Evans. Phase transitions in one-dimensional nonequilibrium systems. *Braz. J. Phys*, 30:42, 2000.

[32] Wojbor A. Woyczynski. *Burgers-KPZ Turbulence: Göttingen Lectures*. Springer-Verlag, 1998.

[33] M. R. Evans and R. A. Blythe. Nonequilibrium dynamics in low dimensional systems. *Physica A*, 313:110.

[34] A. L. Barabasi and E. H Stanley. *Fractal Concepts in a Surface Growth*. Cambridge University Press, 1995.

[35] F. Family and T. Vicsek. Scaling of the active zone in the eden process on percolation networks and the ballistic deposition model. *J. Phys. A.*, 18:L75–L81, 1985.

[36] Raymond Kapral. Multiparticle collision dynamics: Simulation of complex systems on mesoscales. *Adv. in Chem. Phys.*, 140, 2008.

[37] N. Metropolis. The beginning of the monte carlo method. *Los Alamos Science Special Issue*, 1987.

[38] Original press release 1 for eniac computer, February 1946.

[39] Nicholas Metropolis, Arianna W. Rosenbluth, Marshall N. Rosenbluth, Augusta H. Teller, and Edward Teller. Equations of state calculations by fast computing machines. *J. Chem. Phys.*, 21(6):1087, 1953.

[40] W. K. HASTINGS. Monte carlo sampling methods using markov chains and their applications. *Biometrika*, 1970(57):97–109, 1970.

[41] Konstantin S. Turitsyn, Michael Chertkov, and Marija Vucelja. Irreversible monte carlo algorithms for efficient sampling. *Physica D*, 2008.

[42] Daan Frenkel. Speed-up of monte carlo simulations by sampling of rejected states. *PNAS*, 101(51):17571–17575, 2004.

[43] Chantal Valeriani, Rosalind J. Allen, Marco J. Morelli, Daan Frenkel, and Pieter Rein ten Wolde. Computing stationary distributions in equilibrium and nonequilibrium systems with forward flux sampling. *J. Chem. Phys.*, 127(114109), 2007.

[44] A. P. J. Jansen. An introduction to monte carlo simulations of surface reactions. *arXiv: 0303028v1*, 2008.

[45] A. B. Bortz, M. H. Kalos, and J. L. Lebowitz. A new algorithm for monte carlo simulation of ising spin systems. *J. Comp. Phys.*, 17:10, 1975.

[46] Daniel T. Gillespie. A general method for numerically simulating the stochastic time evolution of coupled chemical reactions. *Journal of Computational Physics*, 22(4), 1976.

[47] M.A. Novotny. Monte carlo algorithms with absorbing markoc chains: Fast local algorithms for slow dynamics. *Phys. Rev. Lett.*, 74(1), January 1995.

[48] Rosalind J. Allen, Daan Frenkel, and Pieter Rein ten Wolde. Simulating rare events in equilibrium or nonequilibrium stochastic systems. *J. Chem. Phys.*, 124(024102), 2006.

[49] Kristen A. Fichthorn and W. H. Weinberg. Theoretical foundations of dynamical mote carlo simulations. *J. Chem. Phys.*, 95(2), 1991.

[50] D. Maes and C. Van den Broeck. Discrete versus continuous-time random walks. *J. Stat. Phys.*, 50(5/6).

[51] Ariel Lubelski, Igor M. Sokolov, and Joseph Klafter. Nonergodicity mimics inhomogeneity in single particle tracking. *Phys. Rev. Lett.*, 100(250602), 2008.

[52] Yasmine Meroz adn Igor M. Sokolov and Joseph Klafter. Subdiffusion of mixed origins: When ergodicity and nonergodicity coexist. *Phys. Rev. E.*, 81:010101(R), 2010.

[53] S. C. Ying, I. Vattulainen, J. Merikoski, T. Hjelt, and T. Ala-Nissila. Memory expansion for diffusion coefficients. *Phys. Rev. B.*, 58(2170), 1998.

[54] A.-L. Barabasi. The origin of bursts and heavy tails in human dynamics. *Nature*, 435:207, 2005.

[55] Alvaro Corral. Local distributions and rate fluctuations in a unified scaling law for earthquakes. *Phys. Rev. E.*, 68(035102(R)), 2003.

[56] Per Bak, Kim Christensen, Leon Danon, and Tim Scanlon. Unified scaling law for earthquakes. *Phys. Rev. Lett.*, 88:178501, 2002.

[57] K-I. Goh and A.-L. Barabasi. Burstiness and memory in complex systems. *EPL*, 81(48002), February 2008.

[58] C. Godreche and J. M. Luck. Dynamics of the condensate in zero-range processes. *J. Phys. A*, 38:7215, 2005.

[59] M. Bauer, A. Mougin, J. P. Jamet, V. Repain, J. Ferre, R. L. Stamps, H. Bernas, and C. Chappert. Deroughening of domain wall pairs by dipolar repulsion. *Phys.Rev.Lett.*, 94(207211), 2005.

[60] William Feller. *An introduction to Probability Theory and Its Applications*, volume 2. John Wiley Sons, Inc., 1966.

[61] M. Lax and H. Scher. Renewal theory and ac conductivity in random sructures. *Phys. Rev. Lett.*, 39:781–4, 1977.